communications earth & environment

ARTICLE

https://doi.org/10.1038/s43247-022-00627-y OPEN

Temperature is a better predictor of stable carbon isotopic compositions in marine particulates than dissolved CO_2 concentration

Qianqian Liu [1], Selvaraj Kandasamy [1,2✉], Weidong Zhai [3], Huawei Wang[1], Yoganandan Veeran[4], Aiguo Gao[1] & Chen-Tung Arthur Chen [5]

The stable carbon isotopic composition of marine particulate organic matter ($\delta^{13}C_{POM}$) varies with source and environmental conditions. Dissolved carbon dioxide (CO_2) concentration is thought to influence $\delta^{13}C_{POM}$ more than temperature, but this relationship is poorly constrained in marginal seas. Here we present $\delta^{13}C_{POM}$, hydrographic and carbonate system variables at the deep chlorophyll maxima of the southern Yellow Sea in late summer 2017. We find $\delta^{13}C_{POM}$ values varied between stable and cyclonic gyre regions, but indicated autochthonous organic matter production and were more strongly correlated with temperature than dissolved CO_2 concentration throughout. We find that the relationship between temperature and $\delta^{13}C_{POM}$ was independent of CO_2 concentration, whereas the relationship between $\delta^{13}C_{POM}$ and CO_2 concentration was dependent on temperature also being correlated with CO_2 concentration. We suggest that temperature is the primary determinant of marine $\delta^{13}C_{POM}$ due to temperature-dependent metabolism in phytoplankton, irrespective of inorganic carbon acquisition mode.

[1] Department of Geological Oceanography and State Key Laboratory of Marine Environmental Science, College of Ocean and Earth Sciences, Xiamen University, Xiamen, China. [2] Department of Geology, School of Earth System Science, Central University of Kerala, Periye, Kasaragod, India. [3] Southern Marine Science and Engineering Guangdong Laboratory (Zhuhai), Zhuhai, China. [4] Department of Marine Science, Bharathidasan University, Tiruchirappalli, India. [5] Department of Oceanography, National Sun Yat-Sen University, Kaohsiung, Taiwan. ✉email: selvaraj@xmu.edu.cn

Suspended particulate organic matter (POM) in seawater is a key component of the biological pump which transfers the upper ocean photosynthesized organic matter to the deep sea[1,2]. Stable carbon isotopic composition ($\delta^{13}C$) of the bulk POM ($\delta^{13}C_{POM}$) has long been used to evaluate proportions of marine-derived versus terrestrial POM fractions in coastal oceans[3–5], which are disproportionately important to ocean carbon cycles and budgets[6–8]. However, large variations of $\delta^{13}C$ (−9 to −35‰) naturally occur in marine phytoplankton ($\delta^{13}C_{phyto}$) in the modern ocean[9–11]. These values severely overlap with $\delta^{13}C$ of terrestrial plants-derived OM (−37 to −20‰ of C3 plants[12] and −14 to −11‰ of C4 plants[13]). The widely varied $\delta^{13}C_{phyto}$ are increasingly understood to be a function of environmental variables (pH, temperature, inorganic carbon concentration, and its $\delta^{13}C$ value, nutrient availability, light intensity, and day length) under which the OM was synthesized[11,14,15] and the phytoplankton cell physiology, including cell size, growth rate[16–19], and inorganic carbon acquisition mode (passive diffusion versus active uptake or CO_2 concentrating mechanisms, i.e., CCMs)[20–23]. The widespread CCMs in marine phytoplankton are processes of increasing the CO_2 level at the site of Rubisco through transporters and carbonic anhydrases (CAs), which accelerate the otherwise slow interconversion between HCO_3^- and CO_2[24–26]. The possible influences of biochemical CCMs involving C4-type photosynthesis on $\delta^{13}C_{phyto}$ have been suggested in some species of marine phytoplankton[27,28] but not yet proven[29,30]. Not all of the factors are necessarily relevant under natural conditions in the field, and only a few are likely to exert primary control on $\delta^{13}C_{phyto}$ at most times and location[31]. Although the exact biological processes determining the wide $\delta^{13}C_{phyto}$ ranges are still under debate, in the inferred absence of a major contribution of terrestrial OM to the oceanic POM, the changes of $[CO_2aq]$ have been proposed as the principal determinant of $\delta^{13}C_{POM}$ variability over relatively large areas across the global ocean, where inverse correlations between $\delta^{13}C_{POM}$ and $[CO_2aq]$ were commonly observed[32–34]. On the other hand, due mainly to the well-defined relationship between CO_2 solubility and temperature[35], strong positive correlations of temperature and oceanic $\delta^{13}C_{POM}$[36,37] have long been considered to be resulting from the temperature effects on CO_2 availability[38–42].

Hence, a better understanding of the scales and mechanisms of the marine endmember $\delta^{13}C_{POM}$ variations is an essential prerequisite for the reliable and effective use of this proxy. However, limited observations result in poorly constrained marine end member $\delta^{13}C_{POM}$ in marginal seas, particularly in the southern Yellow Sea (SYS). The SYS is known as a large dynamic marine ecosystem surrounded by China and South Korea[43–45] (Fig. 1a). The deep chlorophyll maxima (DCM) layer in the SYS[46,47], as the general case in the global coastal oceans, forms a substantial part of the annual primary production and export productivity[47–49]. The DCM layer, identified by a pronounced peak in the vertical profiles of chlorophyll (Chl) fluorescence, is a distinct feature of stratified waters that commonly formed between the nutrient-poor, light-replete upper mixed layer and a nutrient-rich, light-limited bottom mixed layer[50–52]. Specifically, during stratified seasons in the SYS, the production within the surface mixed layer is limited as nutrients are depleted due to the consumption by prior spring bloom[53,54]. By contrast, the primary producers at the DCM layer can access nutrients from the bottom water, which is enriched in nutrients due to regeneration processes. For the refinement of marine endmember $\delta^{13}C_{POM}$ in the SYS, it is of particular interest, therefore, to investigate the $\delta^{13}C_{POM}$ at the DCM layer of the SYS. In addition, investigating $\delta^{13}C_{POM}$ in such a dynamic oceanic regime is helpful to better understand the environmental regulation of the oceanic $\delta^{13}C_{POM}$. In fact, previous studies on the mechanisms of $\delta^{13}C_{POM}$ variations have mostly focused on the surface ocean[33,55–57]. Investigation on the $\delta^{13}C_{POM}$ was rarely carried out in the subsurface water[58], such as the DCM layer[59]. Recently, Close and Henderson[60] compiled data from published sources reporting $\delta^{13}C_{POM}$ values for the upper 250 m of open ocean. They demonstrated that $\delta^{13}C_{POM}$ values in the lower euphotic zone, on average, are 1.4‰ lower than those in the upper euphotic zone. This pattern may suggest that the marine endmember $\delta^{13}C_{POM}$, or at least $\delta^{13}C_{POM}$ at the DCM layer, cannot be simply represented by surface $\delta^{13}C_{POM}$.

Here, we concurrently measure Chl *a*, particulate organic carbon (POC) and nitrogen (PN) concentrations and $\delta^{13}C_{POM}$ along with hydrological parameters (e.g., temperature and salinity), and dissolved inorganic carbon (DIC) and total alkalinity (TAlk) (to calculate $[CO_2aq]$) at DCM layers of the SYS. Our data confirm that the POM at the DCM layer is predominantly from marine production, of which the $\delta^{13}C_{POM}$ are widely varied, and that the importance of different phytoplankton communities in two of the contrasting oceanographic areas within the SYS in shaping the $\delta^{13}C_{POM}$-temperature relationships is evident. Moreover, we find that the previously hypothesized inverse relationship between $\delta^{13}C_{POM}$ and $[CO_2aq]$ occurs only when $[CO_2aq]$ is temperature-dependent. When $[CO_2aq]$ is deviating from the temperature-constrained value, then $\delta^{13}C_{POM}$ is less related to $[CO_2aq]$ but still strongly correlated with temperature. This is apparent that $\delta^{13}C_{POM}$ is associated more with temperature than with CO_2aq level in which $\delta^{13}C_{POM}$ is produced. A revisit of studies concluding a general inverse relationship between $\delta^{13}C_{POM}$ and $[CO_2aq]$ strongly supports this view. We provide a mechanistic explanation that reconciles the apparent differences in the trends of $\delta^{13}C_{POM}$-temperature relationships (positive and negative) and reveals that differential temperature scaling on processes regulating $\delta^{13}C_{POM}$ values provides a mean to distinguish between the relative importance of factors on $\delta^{13}C_{POM}$ variations. In addition, our findings do not support a direct effect of $[CO_2aq]$ on $\delta^{13}C_{POM}$ variations but point to a shift in the regulation of CCMs activity and, consequently, the predominance of passive diffusion or efficient CCMs. Given that the $[CO_2aq]$ in large areas of the present-day ocean is higher than the critical 10 μmol/L[14,16,18,61], the increasing CO_2 in the future may not be very effective on carbon assimilation and, therefore, $\delta^{13}C_{POM}$ in the oceanic ecosystem, especially in high latitude areas and subsurface water (e.g., DCM layer).

Results and discussion

Dynamic oceanographic conditions. The hydrological profiles clearly show the presence of a bottom cold water dome at the central region of the SYS (Fig. 1a, b), the so-called Yellow Sea Cold Water Mass (YSCWM), which is a remnant of previous winter water that developed due to stratification from late spring to autumn[62]. The YSCWM acts as a large reservoir of both nutrients and $[CO_2aq]$ due to the remineralization of eutrophication produced OM during spring bloom[63,64]. The DCM layer in most locations is positioned within or at the bottom of the thermocline (Fig. 1b). Temperature of seawater in the DCM layer ranges broadly from 8.6 to 25.1 °C (on average 15.8 ± 4.7 °C; Supplementary Data 1), and it is distinctly lower than the surface water (22.9–27.1 °C, on average 25.0 ± 0.9 °C) (Fig. 1c). The location of DCM in the SYS was also found within the euphotic zone and at the upper part of nitracline[47]. According to the published nutrient data from the same cruise in the present study[65], the dissolved inorganic nitrogen ($DIN = NO_3^- + NO_2^- + NH_4^+$, 0.2–13.7 μmol kg^{-1}) and soluble reactive phosphorus concentrations (P, 0.1–1.0 μmol kg^{-1}), essential macronutrients for phytoplankton growth, are relatively high at the DCM layer of the SYS (Supplementary Fig. 1). Even though the

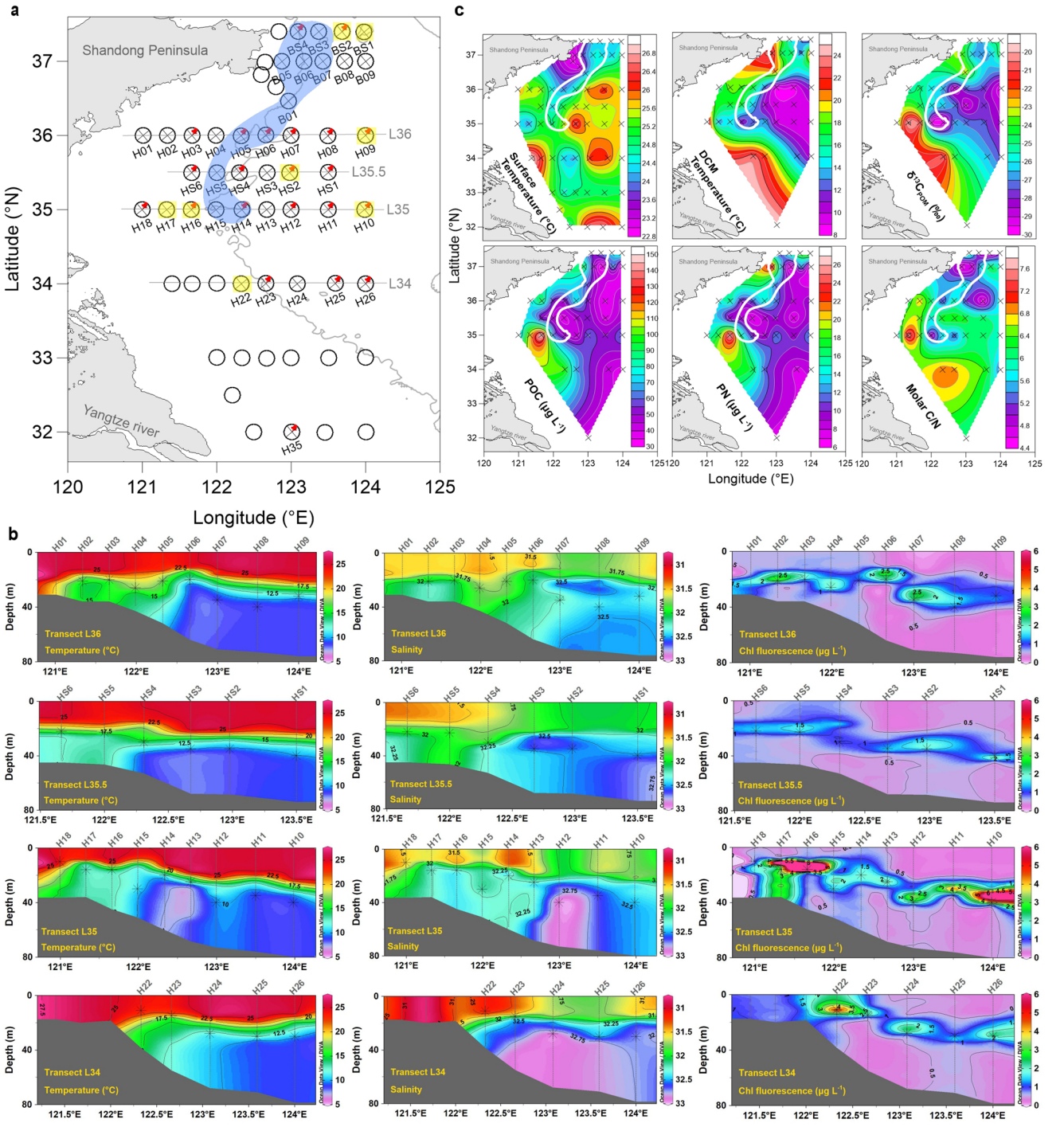

Fig. 1 Study area and spatial distribution of the hydrological and biogeochemical parameters. a Sample location in the southern Yellow Sea (SYS). Circles represent the hydrological stations, crosses are stations with distinct deep chlorophyll maxima (DCM) layers, and red pins indicate stations where [CO_{2aq}] in the DCM layer is concurrently obtained. The solid gray line is the 50-m isobath. $\delta^{13}C_{POM}$ in two DCM stations (H01 and H24) will not be discussed further in this study, since the seawater sample at the DCM layer of H01 was not collected, and the filter at H24 contains less than 50 μgC, which will introduce error for the $\delta^{13}C_{POM}$ measurement. **b** Vertical distribution of temperature, salinity, and chlorophyll fluorescence in four latitudinal transects of middle SYS as marked in (**a**). The dark stars indicate the location where suspended particles were collected. The strong stratification and position of the Yellow Sea Cold Water Mass (YSCWM) can be clearly seen from the structures of temperature and salinity. The upwelling fronts in the western boundary of the YSCWM area can be recognized from temperature profiles. Chl fluorescence profiles clearly demonstrate the existence of the DCM layer. Source data for (**b**) is available in Supplementary Data 2. **c** Horizontal distribution of temperature in both surface and DCM layer, and elemental and stable carbon isotopic composition of particulate organic matter in the DCM layer. Note that the DCM is the depth at which the data was collected. The polygon marked by a white line represents the location of the cyclonic gyre.

DIN/P ratio in the seawater varies in a large range (1–21, on average 10 ± 5)[65], the regeneration and assimilation ratio of these two nutrients at the DCM layer of the SYS is constant and close to the traditional Redfield ratio (16)[66] (Supplementary Fig. 1). This divergence results from the fact that mixing, mainly upward supply from deep water[63,64], rather than consumption in situ is the dominant source of nutrient at the DCM layer of the SYS[67]. The DCM layer is absent in the well-mixed shallow coastal area (Fig. 1a, b) and the well-stratified southern SYS (except at station H35 in L32), wherein the presence of buoyant Yangtze River plume strengthened the stratification (Fig. 1c). For the former, the Chl fluorescence shows a nearly constant value from surface to bottom (Fig. 1b), while for the latter, maximum of Chl fluorescence presents in the upper water instead of the subsurface.

Strong upwelling can be clearly identified from the isotherms uplifting toward the coast in the western boundary of the YSCWM, and it can reach the surface, accounting for the surface cold water patches (Fig. 1b, c) and the ventilation of the thermocline there[68]. Uplift of nutrient-rich water from the bottom reservoir was also observed in the western boundary of the YSCWM[45]. The shallow coastal water and the deep YSCWM area are therefore separated by the upwelling fronts (Fig. 1b, c). The horizontal distributions of temperature in surface water and the DCM layer indicate the presence of a temperature front at ~50 m isobath in the western boundary of YSCWM (Fig. 1a, c). A summertime cyclonic gyre has been identified along the temperature front in the subsurface of the SYS in both observational and numerical studies[68]. Indeed, the DCM stations are divided into three groups based on the relationships of $\delta^{13}C_{POM}$ and temperature along with the hydrological conditions (see subsection Temperature Other than [CO_2aq] Dependent $\delta^{13}C_{POM}$ for details). Specifically, these three groups belong to the stable region, which includes stations with relatively stable hydrological structure, cyclonic gyre which is formed by stations in the western boundary of YSCWM (blue polygon), and the remaining that consists of eight isolated dynamic stations (yellow shaded circles (Fig. 1a). Three of these eight stations are in the coastal upwelling region (H16, H17, H22) and three in the deep central area of SYS (H09, H10, HS2), where downwelling was reported[62].

Marine phytoplankton source of POM in the DCM of the SYS. POC and PN are chemically dominating POM. POC here is operationally defined as all combustible, non-carbonate that can be collected on a filter whose pore size is 0.7 μm but can also effectively retain most particles >0.2 μm[2,69]. Hence, POM in our samples potentially contains phytoplankton, zooplankton, heterotrophic bacteria, and terrestrial components. The concentration of POC and PN in the DCM layer of the SYS varies from 27.7 to 150.0 μg L^{-1} (on average 60.1 ± 25.0 μg L^{-1}) and 5.5 to 26.4 μg L^{-1} (12.1 ± 4.8 μg L^{-1}) (Supplementary Data 1), respectively. The spatial distribution of POC and PN concentrations resemble each other, with higher values on the onshore side of the temperature front than that on the offshore side (Fig. 1c). Significant covariations between these two variables are observed, but with differences in regression from the stable region to cyclonic gyre (Fig. 2a). The nearly zero intercepts on PN axis suggest that the measured nitrogen in the suspended POM is mainly in the organic form. This facilitates the molar C/N ratio to distinguish sources of POM from terrestrial plants (>12)[70] to marine plankton (6–9)[65], and bacteria (2.6–4.3)[71]. The low C/N, ranging from 4.5 to 7.7 (5.8 ± 0.8; Supplementary Data 1 and Fig. 1c) observed in the DCM of the SYS, indicates a non-terrestrial source. Most samples show a C/N ratio close to and below the Redfield ratio (Fig. 2a), indicating that the POM is predominantly derived from the marine plankton assemblages[72,73].

The relationships between concentrations of POC and Chl *a* also differ between the stable region and cyclonic gyre (Fig. 2b). Both regressions show large correlation coefficients indicating that a large part of the POM in the DCM layer of the SYS is associated with Chl *a* and so with living phytoplankton[74–76]. The intercept on the POC axis is assumed to represent the non-photosynthetic component of the POM, which includes both living (heterotrophic) and non-living detritus; this fraction is generally high in both stable region and cyclonic gyre (Fig. 2b). Indeed, scanning electron microscope (SEM) images of two stations (H12 and H15) representative of the stable region and cyclonic gyre show that many of the visible phytoplankton cells (main diatom) are broken (Supplementary Figs. 2 and 3). This may explain the considerable amount of detritus from phytoplankton. The Redfield-like C/N indicates most detritus is autochthonous and without degradation, which in general produces a high C/N due to preferential loss of nitrogen (N) over carbon (C) during OM degradation[77,78]. Therefore, the measured POM is mainly of mixed phytoplankton assemblages. Moreover, the average phytoplankton assemblage-specific C/Chl *a* ratios inferred from the slopes of linear regressions between POC and Chl *a* are close to the ratio normally found in phytoplankton in nutrient-rich waters, c. 30[79,80]. In fact, the phytoplankton C/Chl *a* ratio has been reported in a large range (6– > 400) due to influences of environmental factors such as nutrients and light[76,79,81]. The larger C/Chl *a* ratio in the cyclonic gyre (35.9) than in the stable region (28.4) indicates a more efficient photosynthetic activity of phytoplankton inhabiting the DCM layer in the cyclonic gyre[80]. This is consistent with a higher NH_4^+/DIN ratio (Supplementary Fig. 4), as cells grown on NH_4^+ have a higher affinity for CO_2 and increased photosynthetic CO_2-use efficiency than those grown on NO_3^-; this NH_4^+-induced high CO_2 affinity has been thought to be related to induction/activation of CCMs[26,82].

Overall, the stable region and cyclonic gyre are distinguished from one another in terms of two physiological indicators of phytoplankton assemblages: C/N and C/Chl a. This difference is likely a result of variations in phytoplankton community composition associated with distinct hydrological dynamics. It has been reported that picophytoplankton, composed of *Synechococcus* and picoeukaryotes, dominated the phytoplankton community in both cell abundance and carbon biomass (>90%) at the DCM layer of the central SYS (east of 122.5°E)[47], which belongs to the stable region in the present study, but less was known on the phytoplankton species in the cyclonic gyre. Nonetheless, studies in the SYS found convergence effects of temperature fronts on nutrients[83] and biology, such as phytoplankton, zooplankton, bacterioplankton, and anchovy eggs[45,46], suggesting a biological enhancement and potentially high biodiversity in the cyclonic gyre[44]. The ancillary data from SEM imaging indicate that large-celled phytoplankton (mainly diatoms) were clearly visible in the cyclonic gyre (Supplementary Fig. 3), but a very limited amount was observed in the stable region (Supplementary Fig. 2). This abundant diatom along the front current in the cyclonic gyre is consistent with observations and simulations that revealed the predominance of diatom in meso- and submesoscale structures such as fronts[84]. Furthermore, the larger amount of diatom likely accounts for the lower C/N in the cyclonic gyre (4.5–6.2; 5.4 ± 0.6 on average) than that in the stable region (4.5–6.8; 6.0 ± 0.6 on average) (Supplementary Data 1 and Figs. 1c and 2a), because diatom is capable to store large amounts of N[85,86] and may produce a low C/N ratio in NO_3^--replete environments[87]. Note that although the SEM images show that it is difficult to observe picophytoplankton in both stable regions and cyclonic gyre, this cannot faithfully indicate a relatively low concentration of this microbe present in

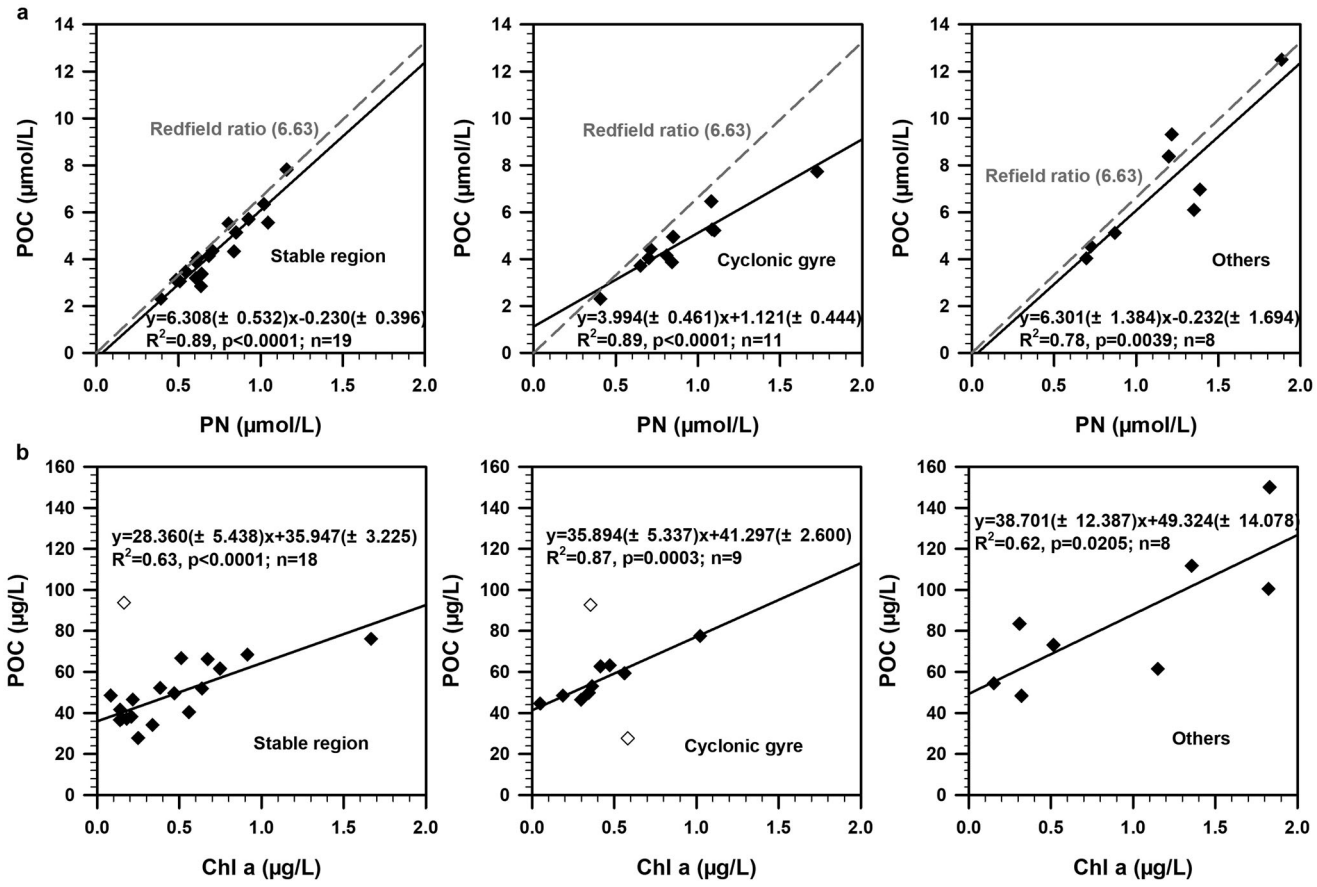

Fig. 2 Marine phytoplankton source of suspended particulate organic matter. a Relationships of POC vs. PN concentrations in three groups of DCM stations. Note that almost all of the data points fall below the line of the Redfield ratio[66]. **b** The covariation of POC and Chl *a* concentrations also indicates the predominant source of marine plankton in the POM at the DCM layer of SYS. Open diamonds in **b** were not included in regressions. The numbers within parentheses of the fitted equation represent standard errors.

the filters. This is because the soft and smaller-sized biology do not tend to preserve well during SEM processing (e.g., freeze-drying and sputter coating)[88]. In contrast, diatoms are protected from heavy alterations during SEM processing by the hard, siliceous cell wall, and are usually still identifiable under SEM observation[89]. Therefore, we tend to suggest that the picophytoplankton (composed of *Synechococcus* and picoeukaryotes)[47] likely dominates in the stable region, while a greater proportion of large-celled phytoplankton (mainly diatom) presents in the cyclonic gyre at the DCM layer of SYS. The low C/N in the picophytoplankton-dominated stable region is clearly different from the reported constant and high C/N (c. 9) of picophytoplankton living in N-depleted environments[87]. Indeed, the biomass C/N has been proposed as an indicator of nutrient supply to phytoplankton[90–92], and the low C/N (< 6.63 of Redfield ratio[66]) observed in the DCM of SYS is indicative of N enrichment. This is well consistent with high stoichiometry of DIN/P by vertical supply from deep water (>16), the main nutrient source of phytoplankton at the DCM layer of SYS, as we discussed earlier in the subsection Dynamic Oceanographic Conditions.

Temperature other than [CO_2aq] dependent $\delta^{13}C_{POM}$. In the inferred absence of major contributions of terrestrial OM, $\delta^{13}C_{POM}$ are representative of $\delta^{13}C_{phyto}$ of locally predominant phytoplankton[33,56,57,93,94], which fuel the entire ocean food web, because heterotrophic processing and decomposition of OM have no or very limited effects on carbon isotopic fractionation[78,95]. Analogous to the large gradient of seawater temperature, $\delta^{13}C_{POM}$ at the DCM layer varies widely from −29.9 to −19.8‰ (average −26.0 ± 2.4) (Supplementary Data 1 and Fig. 1c). Around 10‰ variability of $\delta^{13}C_{POM}$ in such a dynamic marginal sea is quite large, sharing approximately 40% of the 27‰ variation in plankton-derived POM observed globally in the modern ocean[9–11]. A significant linear relationship between $\delta^{13}C_{POM}$ and temperature is observed for the whole data set ($R^2 = 0.39$; $p < 0.0001$; $n = 38$), and the correlation can be improved further when samples in the stable region and cyclonic gyres are separated (Fig. 3a).

Contrary to the hypothesis that the strong positive correlation between $\delta^{13}C_{POM}$ and temperature is resulting from a well-defined solubility relationship between [CO_2aq] and temperature[38–41], we find that the concurrently obtained [CO_2aq] (14.3–31.9 μmol L^{-1}, average: 22.7 ± 4.3 μmol L^{-1}; Supplementary Data 1) doesn't show significant correlation with seawater temperature (Fig. 3b). Rather, temperature sets an upper limit of [CO_2aq] with only five samples in the stable region being [CO_2aq]-saturated with respect to its potential as constrained by temperature (Fig. 3b). This is reasonable because [CO_2aq] can change due to both solubility differences (temperature) and biological acitivity[94]. The hypothesized inverse relationship between $\delta^{13}C_{POM}$ and [CO_2aq] does present in these five samples whose [CO_2aq] follows the temperature-constrained line (Fig. 3b). Meanwhile, the regression line between $\delta^{13}C_{POM}$ and temperature for these five samples (Fig. 3b) is similar to that for the

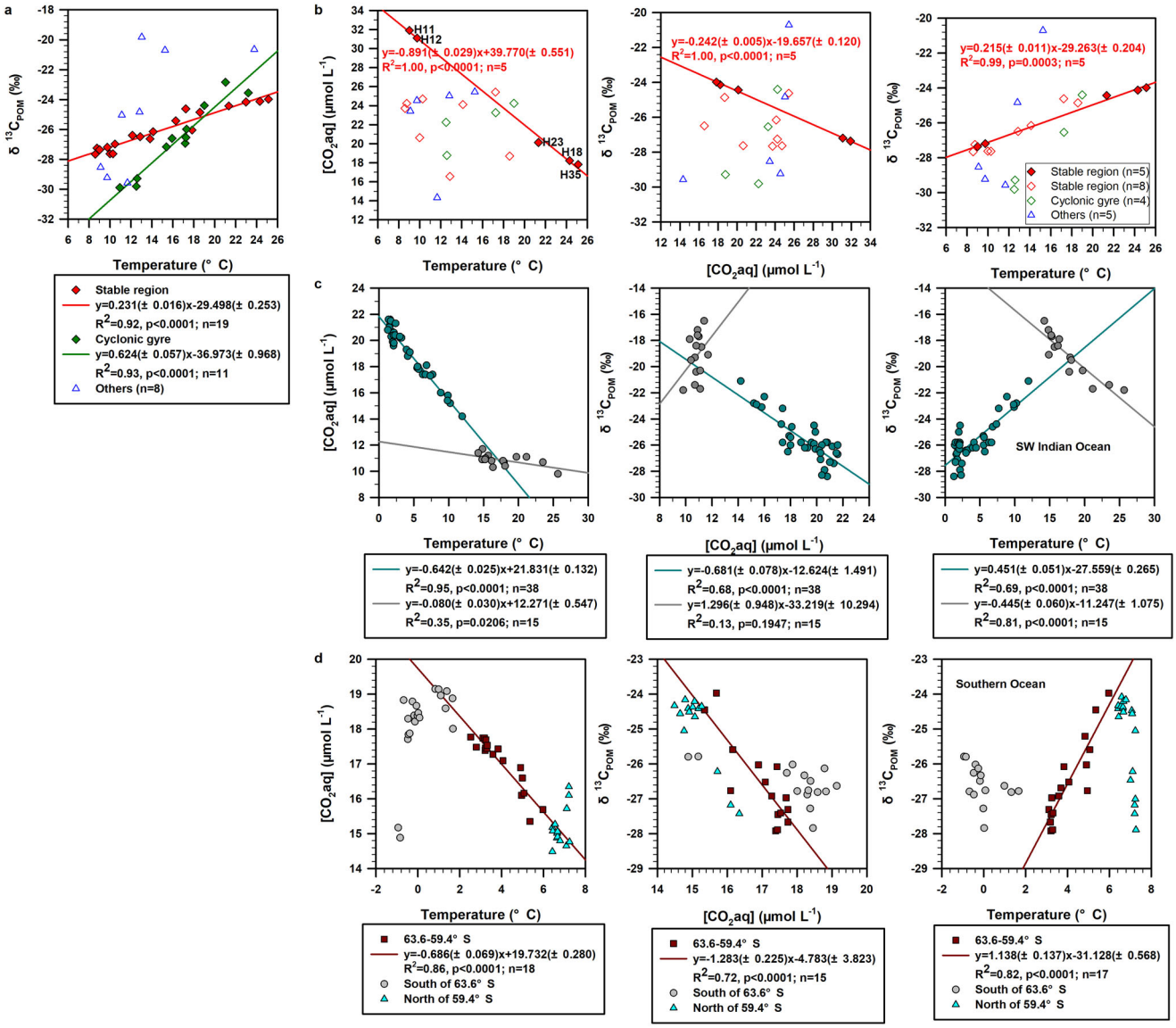

Fig. 3 Association of $\delta^{13}C_{POM}$ with temperature and $[CO_2aq]$. a and **b** are for POM at the DCM layers of the southern Yellow Sea, and **b** is only for stations where concurrent measurement of $[CO_2aq]$ is available (red pins in Fig. 1a). **c**, **d** are same plots for compiled data of POM in the surface water of SW Indian Ocean and Southern Ocean; data in **c**, **d** are derived from Francois et al.[93] and Kennedy and Robertson[94], respectively. $[CO_2aq]$ data derived from Kennedy and Robertson[21] were converted from μmol kg^{-1} to μmol L^{-1} by multiplying 0.001×density (kg m^{-3}). The apparent trend of $\delta^{13}C_{POM}$ with $[CO_2aq]$ in **b** may not reflect the availability of more data in the temperature dataset, since $[CO_2aq]$ wasn't concurrently determined with temperature and $\delta^{13}C_{POM}$ for each station in the DCM of SYS. However, data in the warm SW Indian Ocean (dark gray in **c**) apparently show the presence of a robust linear relationship between $\delta^{13}C_{POM}$ and temperature under a nearly constant $[CO_2aq]$. The numbers within parentheses of the fitted equation represent standard errors.

overall stable region as shown in Fig. 3a. However, $\delta^{13}C_{POM}$ is independent of the external $[CO_2aq]$ for the remaining subset when $[CO_2aq]$ deviates from the temperature-constrained line (Fig. 3b). Thus, it is apparent that the $\delta^{13}C_{POM}$ at the DCM layer of SYS is more closely associated with temperature than with CO_2 levels.

The most striking aspects of our data set are that the previously hypothesized inverse relationship between $\delta^{13}C_{POM}$ and $[CO_2aq]$ occurs only when $[CO_2aq]$ is controlled by temperature, but the robust linear correlation of $\delta^{13}C_{POM}$ and temperature present independently of $[CO_2aq]$ (Fig. 3a, b). Hence, which one, temperature or $[CO_2aq]$, is the direct factor controlling $\delta^{13}C_{POM}$ variation needs to be reconsidered. We are attracted to evaluate whether a temperature-dependent $[CO_2aq]$ is accompanied in previous studies which concluded inverse relationships between $\delta^{13}C_{POM}$ and $[CO_2aq]$ and also evaluate whether the $\delta^{13}C_{POM}$ is significantly correlated with temperature. We only consider studies in which $\delta^{13}C_{POM}$ and $[CO_2aq]$ were concurrently obtained on the same water samples other than calculating $[CO_2aq]$ from pCO_2 in the atmosphere by assuming air-sea equilibrium because the assumption of air–sea equilibrium is not always true for large areas of modern ocean[10,93]. Francois et al.[93] is one of the few earlier field researches in which $[CO_2aq]$ was obtained along with $\delta^{13}C_{POM}$ on the same water samples. Data in Francois et al.[93] showed that although there is a general negative relationship between $\delta^{13}C_{POM}$ and $[CO_2aq]$ in the southwestern (SW) Indian Ocean, these two variables are weakly correlated when $[CO_2aq]$ is nearly constant and low (9.8–11.7 μmol L^{-1}; 10.9 ± 0.5 μmol L^{-1} on average), corresponding to a temperature of > c. 12 °C (Fig. 3c).

To test the temperature effect on [CO_2aq] and $\delta^{13}C_{POM}$, we divided their data into two groups based on temperature: <12 °C (n = 38; green circles in Fig. 3c) and >12 °C (n = 15; dark gray circles in Fig. 3c). They clearly display different regressions of [CO_2aq] against temperature (Fig. 3c). For samples with temperature <12 °C which shows a significant inverse relationship between $\delta^{13}C_{POM}$ and [CO_2aq] ($R^2 = 0.68$, $p < 0.0001$), there is indeed a temperature-dependent [CO_2aq] ($R^2 = 0.95$, $p < 0.0001$) and also a robust correlation of $\delta^{13}C_{POM}$ vs. temperature ($R^2 = 0.69$, $p < 0.0001$) (Fig. 3c). More strikingly but consistent with our data is that as for the temperature >12 °C subset, $\delta^{13}C_{POM}$ are weakly correlated to [CO_2aq] ($R^2 = 0.13$, $p = 0.1947$) but significantly and strongly covaries with temperature ($R^2 = 0.81$, $p < 0.0001$; Fig. 3c), and the [CO_2aq] vs. temperature are weakly correlated ($R^2 = 0.35$, $p = 0.0206$; Fig. 3c). The presence of such a robust linear relationship between $\delta^{13}C_{POM}$ and temperature for data grouped by nearly-constant [CO_2aq] strongly supports temperature having an impact on $\delta^{13}C_{POM}$ values that is independent of the previously hypothesized covariation of [CO_2aq] and temperature. This idea is also supported by the culture experiment of different marine species that revealed an increasingly more negative $\delta^{13}C_{phyto}$ with decreasing temperature under a constant [CO_2aq][96]. Notably, the warm (>12 °C) SW Indian Ocean displays a positive correlation between $\delta^{13}C_{POM}$ and [CO_2aq] other than a previously hypothesized inverse relationship; inverse relationships are observed in the DCM of SYS (Fig. 3a) and in the cold (<12 °C) SW Indian Ocean (Fig. 3c). Meanwhile, contrary to the positive relationships between $\delta^{13}C_{POM}$ and temperature (Fig. 3a, c), a negative covariation is observed in the relatively warm SW Indian Ocean (Fig. 3c). In fact, a similar but weak negative relationship also occurred in the POM at the DCM layers of the East China Sea (ECS), where the $\delta^{13}C_{POM}$ is nearly constant (−23.1 ± 1.5‰) and the seawater temperature is relatively high (19.1–28.2 °C)[59] with [CO_2aq] relatively stable and <12 μmol/L[97]. This contrast will enrich our understanding of the biogeochemical mechanisms involved in the temperature-dependent $\delta^{13}C_{POM}$ variations, and this will be discussed below.

The more sensitive and specific thermal response than [CO_2aq] in $\delta^{13}C_{POM}$ variations is further confirmed by the compiled data set of surface POM from the Southern Ocean[94], which shows a generally weak covariation between the simultaneously obtained $\delta^{13}C_{POM}$ and [CO_2aq] for the whole data set (Fig. 3d). The authors[94] suggested that the large deviations from the hypothesized inverse relation of $\delta^{13}C_{POM}$ and [CO_2aq] are due to the complex hydrological conditions and the associated biological differences, that are more important than [CO_2aq] in controlling the $\delta^{13}C_{POM}$ variations. In this case, we find that temperature can better explain their hypothesis because the plot of $\delta^{13}C_{POM}$ against temperature clearly distinguishes their data set into three hydrologically distinct areas from south to north (Fig. 3d), indicating temperature-induced relative isolation of environments and locally adapted primary producers[98]. This is consistent with the fact that the ecology in the Southern Ocean is highly region-specific; the number of distinct biome zones is divided by fronts[99]. This is also to some extent similar to the case in the DCM of SYS, where two different biomes (i. e. stable region and cyclonic gyre) are distinguished by the different $\delta^{13}C_{POM}$-temperature relationships.

Mechanistic explanations of temperature-dependent $\delta^{13}C_{POM}$. Despite the significance of temperature for many of the patterns and processes in oceanic environments[100,101], we have only a limited understanding of its impact on the stable carbon isotopic composition of marine plankton-produced POM, i.e., $\delta^{13}C_{POM}$. The mechanistic models describing carbon isotopic fractionation during photosynthesis would provide a process-based understanding of community-level $\delta^{13}C_{POM}$ variations. The widely applied models[32,93,102] were originally from terrestrial C3 plants formulated by Farquhar et al.[103], which imply that pure passive diffusion of CO_2aq is the primary mechanism for inorganic carbon transport across the cell membrane. Given the evidence of the prevalence of CCMs in marine phytoplankton and that there is the entry of both CO_2aq and HCO_3^- in CCMs in most algae[25,26], we employ the model that permits the simultaneous uptake of both CO_2aq and HCO_3^- irrespective of the mechanisms by which inorganic carbon enters the cell[14,104]:

$$\delta^{13}C_{\mathrm{phyto}} = \delta^{13}C_{CO_2} - a\varepsilon_{CO_2-HCO_3} - \varepsilon_f + \varepsilon_f \frac{\mu}{F_t} \quad (1)$$

$\delta^{13}C_{CO2}$ is the $\delta^{13}C$ of dissolved CO_2 in the external medium, a likely source of inorganic carbon taken up by phytoplankton. a is the fractional contribution of HCO_3^- to total inorganic carbon uptake (F_t), and $\varepsilon_{CO_2-HCO_3}$ is the equilibrium discrimination between CO_2aq and HCO_3^- ($\varepsilon_{CO_2-HCO_3} = 24.12–9866/T_k$)[105]. ε_f refers to the intrinsic fractionation of Rubisco, which is independent of temperature and varies among species[106,107]. This CO_2aq can be from direct uptake of environmental CO_2aq (passive and/or active), or CA-catalyzed conversion of HCO_3^- to CO_2aq, both ways share similar $\delta^{13}C_{CO2}$ values. This is because there is a fractionation during the dehydration of HCO_3^- by CA[108], which is similar to the fractionation during isotopic equilibration between extracellular HCO_3^- and CO_2aq[105].

Accordingly, the considerable differences in responses of $\delta^{13}C_{POM}$ to changes in temperature (0.23–1.14‰ per °C; Fig. 3a, c, d) among these different oceanic regimes presumably reflect distinct temperature effects on $\delta^{13}C_{CO_2}$ and/or the overall fractionation (ε_p) during photosynthesis relative to CO_2 ($\varepsilon_p \approx \delta^{13}C_{CO_2} - \delta^{13}C_{POM}$), which includes C demand/supply represented by the ratio of growth rate relative to gross C uptake (μ/F_t), and the relative contribution of HCO_3^- to the gross flux of inorganic carbon into the cell. The robust linear correlation of $\delta^{13}C_{POM}$ vs. temperature (Fig. 3a, c, d) implies a constant ε_f, or the same dominant species of phytoplankton across the temperature gradient within each of these five ecosystems since the variation in this term would result in variability in the intercept (but the intercept of $\delta^{13}C_{POM}$ vs. temperature is not solely influenced by ε_f). This is consistent with our analysis of the homogeneous POM sources in the stable region, as well as the cyclonic gyre of the SYS, as discussed above. In addition, it is known that diatom dominates in the cold SW Indian Ocean[93] and Southern Ocean[94], while small-celled phytoplankton such as cyanobacteria, marine prochlorophytes, *Emiliania huxleyi* predominates in the oligotrophic warm SW Indian Ocean[93].

The $\delta^{13}C_{CO_2}$ is commonly calculated from $\delta^{13}C$ of total DIC ($\delta^{13}C_{DIC}$) based on the relationship describing the isotopic fractionation between HCO_3^- (the main form of DIC in seawater) and CO_2aq as a function of temperature ($\varepsilon_{CO_2-HCO_3} = 24.12 - 9866/T_k$)[105]. This calculation neglects the small isotopic fractionation between CO_3^{2-} and HCO_3^- (i.e., $\delta^{13}C_{DIC} = \delta^{13}C_{HCO3}$) and assumes isotopic equilibrium between HCO_3^- and CO_2aq[93]. Unfortunately, the in situ $\delta^{13}C_{DIC}$ was not measured in both the DCM of SYS and Southern Ocean[94]. Similar studies that lack measurement of $\delta^{13}C_{DIC}$ usually assume a constant $\delta^{13}C_{DIC}$ or $\delta^{13}C_{CO2}$[94], which would correspondingly result in a temperature-dependent $\delta^{13}C_{CO_2}$ of c. 0.12[105] or 0 ‰ °C^{-1}. However, the error associated with this approach is difficult to evaluate, and therefore, we are not going to discuss further the temperature effects on $\delta^{13}C_{CO_2}$ and, consequently, the overall

fractionation during carbon fixation in these two areas. Instead, with the measurement of $\delta^{13}C_{DIC}$ by the authors[93], we assess the temperature effects on $\delta^{13}C_{CO_2}$ and consequently ε_p in the SW Indian Ocean. The results show increased $\delta^{13}C_{CO_2}$ of 0.20 and 0.08 ‰ °C^{-1} with increasing temperatures in the cold and warm areas, respectively (Supplementary Fig. 5). The large deviation from 0.12‰ °C^{-1} associated with a constant $\delta^{13}C_{DIC}$ is resulting from the fact that $\delta^{13}C_{DIC}$ in these areas also covary with temperature (0.08 and -0.03 ‰ °C^{-1}, respectively) (Supplementary Fig. 5). Clearly, the response of $\delta^{13}C_{POM}$ to temperature in both warm (0.45 ‰ °C^{-1}) and cold areas (-0.44 ‰ °C^{-1}) (Fig. 3c) cannot be solely accounted for by their temperature-dependent $\delta^{13}C_{CO_2}$. This indicates the important role of temperature in the overall isotopic fractionation, and this is confirmed by the strong relationship of ε_p and temperature (Supplementary Fig. 6). The relative importance of $\delta^{13}C_{CO_2}$ and ε_p on the variations of $\delta^{13}C_{POM}$ are further estimated to be c. 43.9% (18.7%) and 56.1% (81.3%), respectively in the cold (warm) area.

Growth rate (μ), a potentially key variable in the fractionation processes[15,17,18,22], can be evaluated from POC in all five ecosystems, as POC is proportional to growth rate and primary production[33]. The ratio of POC/[CO_2aq], therefore, provides a proxy variable for phytoplankton C demand/supply ratios (μ/F_t). During pure passive diffusion and even with some amount of CCMs, the gross flux of inorganic carbon into the cell is proposed to be proportional to [CO_2aq] in the external medium[14,18,102,109]. With the exception of the warm SW Indian Ocean, the temperature effects on $\delta^{13}C_{POM}$ through associated changes in growth rate are generally weak, as evidenced by the large scatter in the $\delta^{13}C_{POM}$ (and temperature) vs. POC relationships (Fig. 4a–c). Despite this, tight relationships between $\delta^{13}C_{POM}$ and POC/[CO_2aq] are observed in both the *Synechococcus* sp.-dominated stable region of SYS and the diatom-dominated cold SW Indian Ocean. These results underscore the comparable influences of both growth rate and C supply on $\delta^{13}C_{POM}$ in these two regions. However, the chemostat culture studies[18] showed that the fractionation of *Synechococcus* sp. has a much less sensitive relationship (essentially flat, with a small ε_p value) with the ratio of μ/[CO_2aq]. This difference may be attributed to the higher rates of CCMs in N-limited chemostat, fueled by elevated ATP/e$^-$ ratios[15,82], than in the N-enriched, together with a CCM-unfavorable relatively low light intensity, in the DCM of SYS. Because the direct uptake of HCO_3^- is the major mechanism of CCMs in cyanobacteria[110], when HCO_3^- is the major carbon source entering *Synechococcus* sp. cell, the fractionation is expected to remain constant and small[14,111]. This explanation is consistent with Brandenburg et al.[19], who recently found that the ε_p-μ/[CO_2aq] relationships vary significantly between species and groups but also as a result of differences in culture conditions. In addition, the presence of a significant linear correlation between $\delta^{13}C_{POM}$ of mixed phytoplankton assemblages and a proxy variable for C demand/supply (Fig. 4a, b) implies a nearly constant physiological property such as cell size, variation of which confounds the linear relationship between these two variables[18,22]. Consistently, constant C/Chl *a* ratios, a physiological proxy of the average phytoplankton[76,79], are observed in both stable regions of SYS (Fig. 2b) and the SW Indian Ocean (Supplementary Fig. 7). Moreover, a greater proportion of large-celled phytoplankton tends to have higher C demand and thus magnifies the temperature effects on $\delta^{13}C_{POM}$. This may be partly responsible for the larger coefficients in the cyclonic gyre (0.62‰°C^{-1}) relative to the stable region (0.23‰ °C^{-1}) (Fig. 3a). By contrast, the large variability of POC vs. Chl *a* in the Southern Ocean ($R^2 = 0.02$, $p = 0.6009$; Supplementary Fig. 7) provides evidence for the heterogeneity of phytoplankton physiology, which likely caused the absence of a high correlation between $\delta^{13}C_{POM}$ and POC/[CO_2aq] (Fig. 4c). Besides, this phytoplankton diversity can potentially lead to changes in the proportional relationship between POC and growth rate and therefore decreases the reliability of POC/[CO_2aq] to reflect the actual C demand/supply.

Despite the unavailability of temperature effects on $\delta^{13}C_{CO_2}$, the relatively large effect of temperature on $\delta^{13}C_{POM}$ in the Southern Ocean (1.14‰ °C^{-1}; Fig. 3d) indicates that there is a temperature-dependence of the uptake ratio of HCO_3^- to gross C because the $\varepsilon_{CO_2-HCO_3}$ is nearly constant (-11.2 to -11.7‰) within the small temperature gradient (2.5–6.0 °C, Fig. 3d). Specifically, the model equation indicates that this uptake ratio should be a positive linear function of temperature. This assumes that the above model equation captures all of the dominant processes influencing $\delta^{13}C_{POM}$ signatures. Although the effect of temperature changes on the relative contribution of HCO_3^- to total carbon uptake in marine phytoplankton has not been studied well, there are reports showing that this uptake ratio generally increased with decreasing [CO_2aq] in the growth medium, yet strongly differed between species[21,112,113]. The temperature dependence of [CO_2aq] in the Southern Ocean (63.6–59.4°S) (Fig. 3d) well supports the idea that temperature positively covaries with the uptake ratio of HCO_3^- to gross C in diatom in this region. This, in turn, indicates that the observed inverse correlation of $\delta^{13}C_{POM}$ with [CO_2aq] in the Southern Ocean (Fig. 3c) may be caused by the gradual induction of HCO_3^- uptake upon an increase in temperature or a decline in CO_2aq supply. Based on the limited data, no decision can be made about the temperature effects on the uptake ratio of HCO_3^- to gross C in the DCM layers of SYS and the surface water in the SW Indian Ocean.

Generally, below optimum growth temperatures, growth rates of phytoplankton tend to be positively correlated with temperature[101,114]. This trend is due to the enhancement of enzymatic activities of Rubisco and other enzymes related to photosynthesis and depends on the assumption that the ecosystems are of high nutrient availability[92,100,115]. Apparently, the negative linear relationship between $\delta^{13}C_{POM}$ (and ε_p) and temperature in the warm (>12 °C) surface water of SW Indian Ocean (Fig. 3c) is mainly resulting from the decrease of growth rate (and C demand/supply) with increasing temperature (Fig. 4b). The robust inverse relationship between growth rate and temperature can be explained by enzyme kinetics during carbon fixation as described by Michaelis-Menten equation ($\mu = \frac{V_{max} \cdot C}{K_{0.5C} + C}$), in which both maximum C fixation capacity (V_{max}) and half-saturation constants ($K_{0.5}C$) increase with temperature[92]. In the N-starved warm SW Indian Ocean, phytoplankton cells may downregulate the cellular abundance of Rubisco and hence suppress the response of the V_{max} to temperature increase[15,22]. As an alternative strategy to sustain the photosynthesis rate, the CCMs in phytoplankton are therefore essential in the N-limited conditions[15,22], and any changes of growth rate might occur primarily through changes in the CO_2 affinity of Rubisco (i. e. $K_{0.5}C$)[116]. This will lead to a robust inverse correlation of POC and temperature in the N-depleted warm SW Indian Ocean (Fig. 4b). By contrast, in the N-replete systems such as the DCM of SYS and cold SW Indian Ocean, increased cellular Rubisco content may be a viable mechanism to increase V_{max}[22,116]. In addition, the [CO_2aq] in the warm SW Indian Ocean is close to the critical [CO_2aq], that is, roughly 10 μmol L^{-1}, below which the uncatalyzed passive diffusive flux of CO_2 is limited and therefore active CCMs is induced[14,16,18,61]. Moreover, the correlation between $\delta^{13}C_{POM}$ (ε_p) and POC is

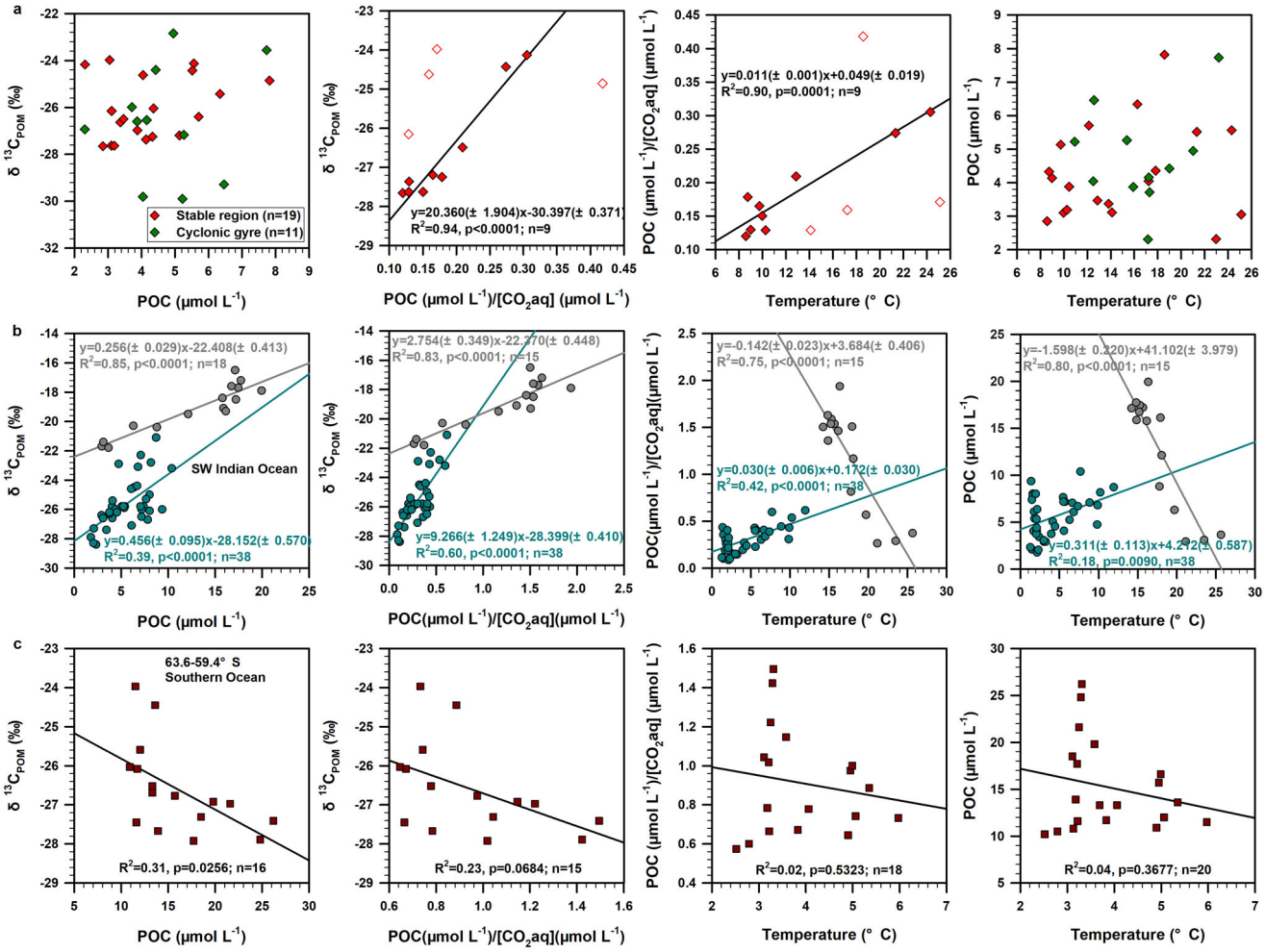

Fig. 4 Mechanisms of temperature-dependent $\delta^{13}C_{POM}$. **a** Correlation of $\delta^{13}C_{POM}$ vs. POC concentrations and $[CO_2aq]$-normalized POC, a proxy variable for carbon (C) demand/supply ratios, as well as $[CO_2aq]$-normalized POC vs. temperature, POC vs. temperature in the DCM of SYS. Due to the small number of $[CO_2aq]$ data available, the specific relationship of $\delta^{13}C_{POM}$ and temperature with POC/$[CO_2aq]$ is not evaluated in the cyclonic gyre of SYS. **b**, **c** Same plots for POM in the surface water of SW Indian Ocean and Southern Ocean for comparison; data in **b**, **c** are derived from Francois et al.[93] and Kennedy and Robertson[94], respectively. Open squares in **a** were not included in the regression. The numbers within parentheses of the fitted equation represent standard errors.

better than either $\delta^{13}C_{POM}$ (ε_p) vs. POC/$[CO_2aq]$ (Fig. 4b and Supplementary Fig. 6) or $\delta^{13}C_{POM}$ (ε_p) vs. $[CO_2aq]$ (Fig. 3c and Supplementary Fig. 6), indicating CO_2-insensitive photosynthesis due likely to a great involvement of active uptake of inorganic carbon in the warm SW Indian Ocean. All these results agree that the transport of DIC into the phytoplankton cell is primarily by CCMs (or efficient CCMs) in the warm SW Indian Ocean that are probably induced by low $[CO_2aq]$ and N-depletion[26,110,117,118]. For phytoplankton possessing efficient CCMs, low temperature reduces the energetic requirement for the CCMs due to a decrease of the CO_2 requirement of Rubisco reflected by $K_{0.5}C$ (or increasing CO_2 affinity of Rubisco) and CO_2 leakage[119]. This may produce an increasing efficiency of CCMs with decreasing temperature and, therefore, a negative relationship of $\delta^{13}C_{POM}$ vs. temperature. By contrast, for marine ecosystems where carbon transport into the cell is dominated by passive diffusion, the decrease of $K_{0.5}C$ at low temperatures would reduce the necessity for CCMs to maintain the supply of CO_2aq to the active site of Rubisco[82]. This downregulation of CCMs with decreasing temperature will result in a positive trend between $\delta^{13}C_{POM}$ and temperature[118]. The linear correlation of $\delta^{13}C_{POM}$ (mainly ε_p) vs. temperature, to some extent, reflects the fine-scale tuning of CCMs due to temperature variations.

In fact, a prominent maximum $\delta^{13}C_{POM}$ in the small-celled phytoplankton dominated and NO_3^- starving warm SW Indian Ocean is coinciding with a maximum in POC (Fig. 4b) and Chl *a* (Supplementary Fig. 7), but with a minimum in $[CO_2aq]$ (Fig. 3c). In addition, by performing a separate linear regression of POC vs. Chl *a* for stations with NO_3^- of 0 μmol L^{-1} in the warm SW Indian Ocean (red color in Supplementary Fig. 7b), we find that the POC is highly correlated with Chl *a* ($R^2 = 0.97$, $p < 0.0001$; $n = 7$), accompanied by a significantly high C/Chl *a* (647) and a very small amount of non-photosynthetic component in POC (9.5 μg L^{-1}) (Supplementary Fig. 7b). This also suggests a phenomenon of phytoplankton bloom termination due to NO_3^- exhaustion. All these results are indicative of phytoplankton bloom termination due to NO_3^- depletion[31,113]. The shift from passive diffusion or inefficient CCMs to efficient CCMs, especially during bloom, is deemed the most effective strategy to overcome carbon limitation and guarantees efficient carbon fixation[20,24,120]. The capability of adjusting the CCMs activity and efficiency to the actual demand in marine phytoplankton may, in part, explain the high productivity related ^{13}C enrichment in the coastal upwelling stations of the SYS (H16: -20.7‰ and H17: -19.8‰; Fig. 1c), which are deviating from the regressions of $\delta^{13}C_{POM}$ against temperature in both stable region and cyclonic gyre (Fig. 3a).

Additionally, due to increasing drain of available CO_2 in ambient water, isotopic disequilibrium between HCO_3^- and CO_2aq would lead to the assimilation of inorganic carbon whose $\delta^{13}C$ has been shifted to that of marine HCO_3^-, thus producing a more positive $\delta^{13}C_{POM}$[121,122]. By comparison, a slow growth rate would thus favor the full expression of isotopic discrimination by Rubisco[119,121].

Despite the primary role of [CO_2aq] in regulating $\delta^{13}C$ of aquatic POM has been questioned, less study provides a parameter that shows systematic effects at least as strong as [CO_2aq]. Based on partial correlation analysis, Wang et al.[123] proposed that pH rather than [CO_2aq] determines the carbon isotopic fractionation during photosynthesis in lake phytoplankton. However, we find through reanalysis that the correlation of carbon isotope fractionation (ε_{HCO_3-POM} and ε_{CO_2-POM}) to temperature in their data is even higher than to pH (Supplementary Fig. 8), which is supported by our partial correlation analysis (Supplementary Table 1). In addition, the correlation of $\delta^{13}C_{POM}$ to temperature is higher than both ε_{HCO_3-POM} and ε_{CO_2-POM} to temperature (Supplementary Fig. 8 and Supplementary Table 1), showing the advantage of temperature in directly regulating the $\delta^{13}C_{POM}$ signals. This may result from the temperature effects on inorganic carbon isotopic values[105]. These results further confirm our idea that the effect of temperature on phytoplankton-produced $\delta^{13}C_{POM}$ variations is stronger than factors that receive far greater attention, e.g., [CO_2aq] and pH. Similarly, recent studies provide evidence that ocean warming rather than acidification controls the coccolithophore calcification[124] and enzyme (e.g., CAs) activities in some marine phytoplankton[125].

In summary, both new data from the DCM layer of the SYS and a reanalysis of selected high-latitude $\delta^{13}C_{POM}$–[CO_2aq] and $\delta^{13}C_{POM}$–temperature paired data indicate that temperature other than [CO_2aq] more strongly determines the oceanic $\delta^{13}C_{POM}$, measured on POM of mixed phytoplankton assemblages. The similarity from very different oceanic settings could be taken as evidence for a common driving force of temperature for determining marine plankton-produced $\delta^{13}C_{POM}$ in natural environments. We find that the predominance of passive diffusion and CCMs, respectively, determines the observed positive and negative $\delta^{13}C_{POM}$-temperature relationships. We, therefore, propose that the role of [CO_2aq] in $\delta^{13}C_{POM}$ variations is mainly to regulate CCMs activity, while temperature-dependent metabolism strongly mediates $\delta^{13}C_{POM}$ irrespective of inorganic carbon acquisition modes. This perspective is helpful to better understand and predict the effect of global warming and ocean acidification on marine ecosystem functioning. It is mechanistically reasonable that temperature imposes such a fundamental and inevitable constraint on the community level $\delta^{13}C_{POM}$ variations, considering that temperature has multiple interactive effects with other properties such as [CO_2aq], pH and nutrient concentrations, and on phytoplankton processes such as growth, physiology, and photosynthesis[98,100,101]. As a consequence, compared to [CO_2aq], the temperature can reduce such phytoplankton-driven variability in deviating their linear relationships with $\delta^{13}C$ of the bulk organic fraction of marine plankton in natural assemblages. However, we are not suggesting that $\delta^{13}C_{POM}$ can be used to reconstruct seawater temperature, because this prediction must assume that the relationship between $\delta^{13}C_{POM}$ and temperature is constant and predictable. Instead, we tend to propose that the strong linear relationship between $\delta^{13}C_{POM}$ and temperature is a phenomenological representation of the impact of temperature on $\delta^{13}C_{POM}$, which encompasses broad physiological differences among taxa adapted to diverse thermal environments[101]. In addition, differential temperature scaling on processes regulating $\delta^{13}C_{POM}$ values provides a mean to distinguish between the relative importance of variation in C demand/supply, $\delta^{13}C_{CO_2}$, and $a\varepsilon_{CO_2-HCO_3}$ on $\delta^{13}C_{POM}$ (and ε_p). Based on the large deviations from the hypothesized inverse relationships of $\delta^{13}C_{POM}$ and [CO_2aq], pioneers[10,93,94] realized that factors linked to intracellular physiological processes could be more important than [CO_2aq] in establishing the marine plankton produced $\delta^{13}C_{POM}$, but the potentially responsible parameters have not been revealed yet. We provide an alternate perspective that temperature principally links intracellular physiological and photosynthetic processes, resulting in a sensitive and specific $\delta^{13}C_{POM}$ response, which can obscure the simple relationship between $\delta^{13}C_{POM}$ and [CO_2aq]. This brings a promising approach to the decades-old problem in marine biogeochemistry.

Future studies with simultaneous measurements of in situ $\delta^{13}C_{DIC}$ and taxon identification on the same water samples of POM, as well as the improved knowledge of the intrinsic fractionation of Rubisco in various species of phytoplankton, are helpful for an in-depth understanding of the mechanisms driving $\delta^{13}C_{POM}$ variability at species and community level in natural environments. Better estimation of $\delta^{13}C_{CO_2}$ by considering isotopic disequilibrium between HCO_3^- and CO_2aq could also greatly improve the distinction of relative impact between [CO_2aq] and processes regulating ε_p on $\delta^{13}C_{POM}$ variations. It is also important to study the $\delta^{13}C_{POM}$ of classified phytoplankton by separating different contributions through a variety of complementary techniques, such as genetic/molecular tools or cell sorting, or size-class sorting using filters with different pore sizes or microscopy. In addition, molecular biomarkers known to be derived from restricted taxonomic sources may also help minimize issues associated with secondary biological processing or terrestrial inputs and therefore improve the likelihood that the measured isotopic signature reflects the fractionation due to photosynthesis by marine phytoplankton rather than some other processes.

Methods

Hydrographic data collection. This investigation was conducted on the Chinese side of the southern Yellow Sea (SYS) (Fig. 1a) between 29 August and 3 September 2017 on the research vessel *Dongfanghong 2*. Hydrological data (temperature and salinity) and Chl fluorescence concentration were measured in situ by a calibrated conductivity-temperature-depth rosette (Sea-Bird SBE 911+) fitted with detectors for Chl fluorescence. The DCM layers were identified from the Chl fluorescence profiles. Seawater samples for suspended POM, DIC, and TAlk were collected from the DCM layers through Niskin bottles mounted on the conductivity–temperature–depth rosette.

POM measurement. Suspended particles for organic carbon and nitrogen, as well as for Chl *a* measurement, were obtained by immediately filtering seawater through 0.7 μm Whatman glass fiber filters (GF/F) under an ultimate pressure of 0.08 MPa to avoid the rupturing of phytoplankton cells. The volume of filtered seawater, 0.95–10.95 L for each filter, depended on the particle contents. In many cases, the amounts of particles on the filters were so high that seawater could not flow through. At least two filters were collected at each site for separate downstream analysis (Chl *a* and POC/PN/$\delta^{13}C_{POM}$). At some stations, filters with different diameters (25 mm and 47 mm) were used, according to the seawater amount shared onboard. All filters were pre-combusted at 450 °C for 4 h in a muffle furnace to remove the background carbon and wrapped in aluminum foil. After filtration, these filters were folded in half without rinsing, and wrapped again in aluminum foil. They were immediately stored at −20 °C in a freezer onboard until shore analysis at the State Key Laboratory of Marine Environmental Science, Xiamen University, where filters with suspended particles, except those for Chl *a* measurement, were firstly freeze-dried by a CHRIST Alpha 1–4 LDplus freezer-drier interfaced to a Vacuubrand RZ 6 vacuum pump.

For Chl *a* analysis, filters of 25 mm diameter were used. The Chl *a* retained on the filters was determined by the non-acidification method[126] using a Turner Trilogy fluorometer available in the Center of Major Experiment and Technology of Xiamen University. The fluorometer was previously calibrated with a Chl *a* standard (Sigma-C6144) by using 90% acetone; the concentration of the standard solution was determined spectrophotometrically (Ultraviolet Spectrometer, model

722) using an extinction coefficient of 87.67 l g^{-1} cm^{-1} at 664 nm against a 90% acetone blank. The filter was removed from the aluminum foil, and the whole filter was placed in the 5 ml centrifuge tube with a screw cap. 3.5 ml of 90% acetone was then added into the centrifuge tube by careful pipetting. These centrifuge tubes were then wrapped with aluminum foil to avoid light and placed in the freezer at −20 °C for 16–20 h. Before analysis, the sample extract was allowed to stand at room temperature for 30 min, and the fluorometer was allowed to warm up for 15 mins. The sample extracts were transferred from centrifuge tubes to the fluorometer cuvette, and the fluorescence of the sample extract was finally measured against a 90% acetone blank. The Chl *a* concentration for each sample was calculated based on the previously calibrated relationship of Chl *a* concentration and fluorescence. The detection limit for Chl *a* is 0.02 μg L^{-1}.

For POC, PN, and $\delta^{13}C_{POM}$ analysis, both 25 mm ($n = 28$) and 47 mm ($n = 10$) filters were employed. These filters were first removed from the aluminum foil. Half of the 47 mm or full 25 mm filter was then placed into the culture dishes, and several drops of 1 N HCl were added to each dish to cover the filter. They were allowed to react for 16 h to remove inorganic carbon (mainly carbonate). The carbonate-free samples were dried in an oven at 50 °C to remove the excess HCl. Then a half (i.e., a quarter of the 47 mm filter) or full (25 mm filter) of the carbonate-free filter, corresponding to 0.75–4.35 L filtered seawater, was then punched and packed in tin capsules. The POC, PN, and $\delta^{13}C_{POM}$ were determined through an elemental analyzer (Elementar Analysensysteme GmbH) interfaced with a PDZ Europa 20–20 isotope ratio mass spectrometer at the Stable Isotope Facility of the University of California Davis in the USA. The stable carbon isotope ratios were presented as per mil deviation from standard-VPDB and expressed as $\delta^{13}C = \left(\frac{(^{13}C/^{12}C)_{sample}}{(^{13}C/^{12}C)_{standard}} - 1\right) \times 1000$. During analysis, samples are interspersed with several replicates of four different laboratory standards (Glutamic Acid, Bovine Liver, Enriched Alanine, and Nylon 6). These laboratory standards have been previously calibrated against international reference materials, including IAEA-600, USGS-40, USGS-41, USGS-42, USGS-43, USGS-61, USGS-64, and USGS-65. A sample's provisional isotope ratio is measured relative to a standard gas peak analyzed with each sample. These provisional values are finalized by correcting the values for the entire batch based on the known values of the included laboratory standards (https://stableisotopefacility.ucdavis.edu/carbon-and-nitrogen-solids). The standard deviation of $\delta^{13}C_{POM}$ was 0.2‰, and the precision decreases when samples contain <100 μgC. Among 38 particulate samples measured in the present study, fourteen contain <100 μgC, but six of these fourteen show >90 μgC, all >67 μgC. Molar C/N ratios of POM were calculated from the measured POC and PN.

DIC and TAlk analysis. Seawater samples for DIC and TAlk analyses were stored in 60 mL borosilicate glass bottles and 140 mL high-density polyethylene bottles, respectively, and were then immediately mixed with 50 μL saturated $HgCl_2$. During DIC sample collection, seawater was overflowed by a full bottom volume, while TAlk samples were collected after several swing-washings without overflowing. These samples were sealed with screw caps and stored at room temperature before further analysis in the platform of Marine Carbon Chemistry in Shandong University. This sampling protocol is slightly different from Dickson et al.[127] guides but has received a favorable evaluation by Huang et al.[128]. It was concluded that there were no differences between the results obtained using our procedure and those derived using the widely adopted sampling procedure recommended by Dickson et al.[127]. The data quality of surface DIC and TAlk of this cruise has been evaluated by comparison between the calculated sea surface fugacity of CO_2 (fCO_2) and the underway measurement of sea surface partial pressure of CO_2 (pCO_2, nearly the same as the fCO_2 in usual sea surface settings)[129]; this was discussed below. These seawater samples were firstly allowed to static sedimentation to obtain the supernatant for DIC and TAlk measurement. For DIC analysis, a commercial analytical system (model AS-C3, Apollo SciTech Inc., USA) was used. Briefly, a DIC sample of 0.5–0.9 mL was injected using a Kloehn® digital syringe pump and acidified with 1.5 mL of 10% analytical-grade phosphoric acid. The extracted gas was quantitatively collected in internal pipes for final determination using an infrared CO_2 detector (model Li-7000, Li-Cor Inc., USA). For TAlk analysis, a water sample of 15–25 mL was determined at 25 °C by the Gran acidimetric titration using a semi-automated titrator (AS-ALK2, Apollo SciTech Inc., USA). During analysis, we used the certified reference materials from Dickson's lab (Batch#156) (https://www.ncei.noaa.gov/access/ocean-carbon-acidification-data-system/oceans/Dickson_CRM/batches.html) for quality assurance, achieving a precision of ±2 μmol kg^{-1}.

The [CO_2aq] was calculated based on pressure, temperature, salinity, and measured DIC and TAlk, using the program CO2SYS.XLS (version 24). The dissociation constants of carbonic acid and for HSO_4^- were used by Millero et al.[130] and Dickson[131], respectively, in the calculation. Phosphate and silicate concentrations required by the program were from measurements that reported by Zheng and Zhai[65]. The calculated [CO_2aq] was finally converted from a unit of μmol kg^{-1} into μmol L^{-1} by multiplying 0.001×density (kg m^{-3}). We also calculated $[CO_2aq]_0$ by the same program, except that the phosphate and silicate concentrations were replaced by zero. The dissolved CO_2 concentrations calculated from these two methods show significant linear correlation ($R^2 = 1.00$, $p < 0.0001$; $n = 21$; Supplementary Fig. 9). By applying this regression equation, we derived the [CO_2aq] of sample HS1, of which the nutrient concentration was not measured.

To assess the quality of the calculated data set, we conducted the underway measurement of pCO_2 and also collected surface seawater for fCO_2 calculation using the same program as [CO_2aq] calculation mentioned above; this surface carbonate data set has been published by Wang and Zhai[129]. The calculated fCO_2 was greater than the field-measured pCO_2 by 14 ± 28 μatm ($n = 40$) on average (mean ± S.D.), indicating less than 5% error relative to the 400 μatm, the approximate air-equilibrated pCO_2 level during our surveys[129]. Note that this is for the surface water, and the error for the DCM sample is expected to be smaller due to the decrease of associated systematic error in subsurface water[129].

SEM imaging. Two filters (0.7 μm/25 mm) representative of the stable region (H12) and cyclonic gyre (H15) were selected to be imaged in the Field Emission SEM (FEI Quanta 650 FEG) in the Center of Major Experiment and Technology of Xiamen University. Particles were evenly distributed on the surface of the filters. Before SEM imaging, the selected filters were first cut in half and trimmed to fit the sample stub. The conductive tap was then used to mount the filter on the sample stub and to create a contact between these two. After sputtering with gold for 120 s, the sample stub was inserted into the sample holder in the vacuum chamber. SEM images were recorded at magnifications ranging from 127× to 74,059×.

Reporting summary. Further information on research design is available in the Nature Portfolio Reporting Summary linked to this article.

Data availability

All data used in this paper are available in Supplementary Data 1 and Supplementary Data 2. Both data files are deposited in the public repository, Figshare, at: https://doi.org/10.6084/m9.figshare.21393261. The data compiled from published papers are available via their respective cited references.

Received: 3 March 2022; Accepted: 14 November 2022;
Published online: 01 December 2022

References

1. Boyd, P. W., Claustre, H., Levy, M., Siegel, D. A. & Weber, T. Multi-faceted particle pumps drive carbon sequestration in the ocean. *Nature* **568**, 327–335 (2019).
2. Kharbush, J. J. et al. Particulate organic carbon deconstructed: molecular and chemical composition of particulate organic carbon in the ocean. *Front. Mar. Sci.* **7**, 518 (2020).
3. Fry, B. & Sherr, E. B. $\delta^{13}C$ measurements as indicators of carbon flow in marine and freshwater ecosystems. in *Stable Isotopes in Ecological Research* (eds Rundel, P. W., Ehleringer, J. R. & Nagy, K. A.) (Springer, 1989).
4. Thornton, S. F. & McManus, J. Application of organic carbon and nitrogen stable isotope and C/N ratios as source indicators of organic matter provenance in estuarine systems: evidence from the Tay Estuary, Scotland. *Estuar. Coast. Shelf Sci.* **38**, 219–233 (1994).
5. Liénart, C. et al. Dynamics of particulate organic matter composition in coastal systems: a spatio-temporal study at multi-systems scale. *Progr. Oceanogr.* **156**, 221–239 (2017).
6. Hofmann, E. E. et al. Modeling the dynamics of continental shelf carbon. *Annu. Rev. Mar. Sci.* **3**, 93–122 (2011).
7. Bauer, J. E. et al. The changing carbon cycle of the coastal ocean. *Nature* **504**, 61–70 (2013).
8. Dai, M. H. et al. Carbon fluxes in the coastal ocean: synthesis, boundary processes, and future trends. *Annu. Rev. Earth Planet. Sci.* **50**, 593–626 (2022).
9. Descolas-gros, C. & Fontugne, M. Stable carbon isotope fractionation by marine phytoplankton during photosynthesis. *Plant Cell Environ* **13**, 207–218 (1990).
10. Goericke, R. & Fry, B. Variations of marine plankton $\delta^{13}C$ with latitude, temperature, and dissolved CO_2 in the world ocean. *Glob. Biogeochem. Cycles* **8**, 85–90 (1994).
11. Deuser, W. G., Degens, E. T. & Guillard, R. R. L. Carbon isotope relationships between plankton and sea water. *Geochim. Cosmochim. Acta* **32**, 657–660 (1968).
12. Kohn, M. J. Carbon isotope compositions of terrestrial C3 plants as indicators of (paleo)ecology and (paleo)climate. *Proc. Natl. Acad. Sci. USA* **107**, 19691–19695 (2010).
13. Cernusak, L. A. et al. Environmental and physiological determinants of carbon isotope discrimination in terrestrial plants. *New Phytol.* **200**, 950–965 (2013).
14. Burkhardt, S., Riebesell, U. & Zondervan, I. Effects of growth rate, CO_2 concentration, and cell size on the stable carbon isotope fractionation in marine phytoplankton. *Geochim. Cosmochim. Acta* **63**, 3729–3741 (1999).

15. Riebesell, U., Burkhardt, S., Dauelsberg, A. & Kroon, B. Carbon isotope fractionation by a marine diatom: dependence on the growth-rate-limiting resource. *Mar. Ecol. Prog. Ser.* **193**, 295–303 (2000).
16. Laws, E. A., Popp, B. N., Bidigare, R. R., Kennicutt, M. C. & Macko, S. A. Dependence of phytoplankton carbon isotopic composition on growth rate and [CO_2aq]: Theoretical considerations and experimental results. *Geochim. Cosmochim. Acta* **59**, 1131–1138 (1995).
17. Rau, G. H., Riebesell, U. & Wolf-Gladrow, D. A model of photosynthetic ^{13}C fractionation by marine phytoplankton based on diffusive molecular CO_2 uptake. *Mar. Ecol. Prog. Ser.* **133**, 275–285 (1996).
18. Popp, B. N. et al. Effect of phytoplankton cell geometry on carbon isotopic fractionation. *Geochim. Cosmochim. Acta* **62**, 69–77 (1998).
19. Brandenburg, K. M., Rost, B., Van de Waal, D. B., Hoins, M. & Sluijs, A. Physiological control on carbon isotope fractionation in marine phytoplankton. *Biogeosciences* **19**, 3305–3315 (2022).
20. Sharkey T. D. & Berry J. A. Carbon isotope fractionation of algae as influenced by an inducible CO_2 concentrating mechanism. in *Inorganic Carbon Uptake by Aquatic Photosynthetic Organisms* (eds Lucas W. J. & Berry J. A.) 389–401 (American Society of Plant Physiologists, 1985)
21. Raven, J. A. et al. Mechanistic interpretation of carbon isotope discrimination by marine macroalgae and seagrasses. *Funct. Plant Biol.* **29**, 355–378 (2002).
22. Cassar, N., Laws, E. A. & Popp, B. N. Carbon isotopic fractionation by the marine diatom *Phaeodactylum tricornutum* under nutrient- and light-limited growth conditions. *Geochim. Cosmochim. Acta* **70**, 5323–5335 (2006).
23. Wikes, E. & Pearson, A. A general model for carbon isotopes in red-lineage phytoplankton: interplay between unidirectional processes and fractionation by RubisCO. *Geochim. Cosmochim. Acta* **265**, 163–181 (2019).
24. Rost, B., Riebesell, U. & Sultemeyer, D. Carbon acquisition of marine phytoplankton: effect of photoperiod length. *Limnol. Oceanogr.* **5**, 12–20 (2006).
25. Raven, J. A. & Beardall, J. The ins and outs of CO_2. *J. Exp. Bot.* **67**, 1–13 (2016).
26. Giordano, M., Beardall, J. & Raven, J. A. CO_2 concentrating mechanisms in algae: mechanisms, environmental modulation, and evolution. *Annu. Rev. Plant Biol.* **56**, 99–131 (2005).
27. Reinfelder, J. R., Kraepiel, A. M. L. & Morel, F. M. M. Unicellular C4 photosynthesis in a marine diatom. *Nature* **407**, 996–999 (2000).
28. Reinfelder, J. R., Milligan, A. J. & Morel, F. M. M. The role of the C4 pathway in carbon accumulation and fixation in a marine diatom. *Plant Physiol* **135**, 2106–2111 (2004).
29. Clement, R., Dimnet, L., Maberly, S. C. & Gontero, B. The nature of the CO_2-concentrating mechanisms in a marine diatom, *Thalassiosira pseudonana*. *New Phytol.* **209**, 1417–1427 (2015).
30. Pierella Karlusich, J. J., Bowler, C. & Biswas, H. Carbon dioxide concentration mechanisms in natural populations of marine diatoms: insights from Tara Oceans. *Front. Plant Sci.* **12**, 657821 (2021).
31. Kukert, H. & Riebesell, U. Phytoplankton carbon isotope fractionation during a diatom spring bloom in a Norwegian fjord. *Mar. Ecol. Prog. Ser.* **173**, 127–137 (1998).
32. Rau, G. H., Takahashi, T., Desmarais, D. J., Repeta, D. J. & Martins, J. H. The relationship between $\delta^{13}C$ of organic matter and [CO_2aq] in ocean surface water: data from a JGOFS site in the northeast Atlantic Ocean and a model. *Geochim. Cosmochim. Acta* **56**, 1413–1419 (1992).
33. Hofmann, M. et al. Stable carbon isotope distribution of particulate organic matter in the ocean: a model study. *Mar. Chem.* **72**, 131–150 (2000).
34. Young, J. N., Bruggeman, J., Rickaby, R. E. M., Erez, J. & Conte, M. Evidence for changes in carbon isotopic fractionation by phytoplankton between 1960 and 2010. *Glob. Biogeochem. Cycles* **27**, 505–515 (2013).
35. Weiss, R. F. Carbon dioxide in water and seawater: the solubility of a non-ideal gas. *Mar. Chem.* **2**, 203–215 (1974).
36. Sackett, W. M., Eckelmann, W. R., Bender, M. L. & Bé, A. W. H. Temperature dependence of carbon isotope composition in marine plankton and sediments. *Science* **148**, 235–237 (1965).
37. Fontugne, M. R. & Duplessy, J. C. Organic carbon isotopic fractionation by marine plankton in the temperature range −1 to 31 °C. *Oceanol. Acta* **4**, 85–90 (1981).
38. Rau, G. H., Takahashi, T. & Desmarais, D. J. Latitudinal variations in plankton $\delta^{13}C$: implications for CO_2 and productivity in past oceans. *Nature* **341**, 516–518 (1989).
39. Savoye, N. et al. Dynamics of particulate organic matter $\delta^{15}N$ and $\delta^{13}C$ during spring phytoplankton blooms in a macrotidal ecosystem (Bay of Seine, France). *Mar. Ecol. Prog. Ser.* **255**, 27–41 (2003).
40. Lourey, M. J., Trull, T. W. & Tilbrook, B. Sensitivity of $\delta^{13}C$ of Southern Ocean suspended and sinking organic matter to temperature, nutrient utilization, and atmospheric CO_2. *Deep Sea Res. Part I* **51**, 281–305 (2004).
41. Lara, R. J., Alder, V., Franzosi, C. A. & Kattner, G. Characteristics of suspended particulate organic matter in the southwestern Atlantic: influence of temperature, nutrient and phytoplankton features on the stable isotope signature. *J. Mar. Syst.* **79**, 199–209 (2010).
42. Soares, M. A. et al. Latitudinal $\delta^{13}C$ and $\delta^{15}N$ variations in particulate organic matter (POM) in surface waters from the Indian ocean sector of Southern Ocean and the Tropical Indian Ocean in 2012. *Deep Sea Res. Part II* **118**, 186–196 (2015).
43. Belkin, I. M., Cornillon, P. C. & Sherman, K. Fronts in large marine ecosystems. *Prog. Oceanogr.* **81**, 223–236 (2009).
44. Belkin, I. M. Remote sensing of ocean fronts in marine ecology and fisheries. *Remote Sens* **13**, 883 (2021).
45. Wei, Q. S. et al. Seasonally chemical hydrology and ecological responses in frontal zone of the central southern Yellow Sea. *J. Sea Res.* **112**, 1–12 (2016).
46. Fu, M. Z. et al. Phytoplankton biomass size structure and its regulation in the Southern Yellow Sea (China): Seasonal variability. *Cont. Shelf Res.* **29**, 2178–2194 (2009).
47. Fu, M. Z. et al. Structure, characteristics and possible formation mechanisms of the subsurface chlorophyll maximum in the Yellow Sea Cold Water Mass. *Cont. Shelf Res.* **165**, 93–105 (2018).
48. Hickman, A. E. et al. Primary production and nitrate uptake within the seasonal thermocline of a stratified shelf sea. *Mar. Ecol. Prog. Ser.* **463**, 39–57 (2012).
49. van Leeuwen, S. M., van der Molen, J., Ruardij, P., Fernand, L. & Jickells, T. Modelling the contribution of deep chlorophyll maxima to annual primary production in the North Sea. *Biogeochemistry* **113**, 137–152 (2013).
50. Cullen, J. J. Subsurface chlorophyll maximum layers: enduring enigma or mystery solved? *Annu. Rev. Mar. Sci.* **7**, 207–239 (2015).
51. Wafar, M., Qurban, M. A., Nazeer, Z. & Manikandan, K. Deep chlorophyll maximum (DCM) in the Red Sea. *Arabian J. Geosci.* **14**, 211 (2021).
52. Cornec, M. et al. Deep chlorophyll maxima in the global ocean: occurrences, drivers and characteristics. *Glob. Biogeochem. Cycles* **35**, e2020GB006759 (2021).
53. Xuan, J. L. et al. Physical processes and their role on the spatial and temporal variability of the spring phytoplankton bloom in the central Yellow Sea. *Acta Ecolo. Sin.* **31**, 61–70 (2011).
54. He, X. Q. et al. Satellite views of the seasonal and interannual variability of phytoplankton blooms in the eastern China seas over the past 14 yr (1998–2011). *Biogeosciences* **10**, 4721–4739 (2013).
55. Oczkowski, A., Kreakie, B., McKinney, R. A. & Prezioso, J. Patterns in stable isotope values of nitrogen and carbon in particulate matter from the Northwest Atlantic continental shelf, from the Gulf of Maine to Cape Hatteras. *Front. Mar. Sci.* **3**, 252 (2016).
56. Henley, S. F. et al. Factors influencing the stable carbon isotopic composition of suspended and sinking organic matter in the coastal Antarctic sea ice environment. *Biogeosciences* **9**, 1137–1157 (2012).
57. Tuerena, R. E. et al. Isotopic fractionation of carbon during uptake by phytoplankton across the South Atlantic subtropical convergence. *Biogeosciences* **16**, 3621–3635 (2019).
58. Winogradow, A., Mackiewicz, A. & Pempkowiak, J. Seasonal changes in particulate organic matter (POM) concentrations and properties measured from deep areas of the Baltic Sea. *Oceanologia* **61**, 505–521 (2019).
59. Liu, Q. Q., Kandasamy, S., Lin, B. Z., Wang, H. W. & Chen, C. T. A. Biogeochemical characteristics of suspended particulate matter in deep chlorophyll maximum layers in the southern East China Sea. *Biogeosciences* **15**, 2091–2109 (2018).
60. Close, H. G. & Henderson, L. C. Open-ocean minima in ^{13}C values of particulate organic carbon in the lower euphotic zone. *Front. Mar. Sci.* **7**, 540165 (2020).
61. Bidigare, R. R. et al. Consistent fractionation of ^{13}C in nature and in the laboratory: growth-rate effects in some haptophyte algae. *Glob. Biogeochem. Cycles* **11**, 279–292 (1997).
62. Su, J. L. & Huang, D. J. On the current field associated with the Yellow Sea Cold Water Mass. *Oceanol. Limnol. Sin.* **26**, 1–7 (1995).
63. Su, N., Du, J. Z., Liu, S. M. & Zhang, J. Nutrient fluxes via radium isotopes from the coast to offshore and from the seafloor to upper waters after the 2009 spring bloom in the Yellow Sea. *Deep Sea Res. Part II* **97**, 33–42 (2013).
64. Wang, X. X. et al. Radon traced seasonal variations of water mixing and accompanying nutrient and carbon transport in the Yellow-Bohai Sea. *Sci. Total Environ.* **784**, 147161 (2021).
65. Zheng, L. & Zhai, W. Excess nitrogen in the Bohai and Yellow seas, China: Distribution, trends, and source apportionment. *Sci. Total Environ.* **794**, 148702 (2021).
66. Redfield, A. C. The biological control of chemical factors in the environment. *Am. Sci.* **46**, 230A–221A (1958).
67. Steele, J. H. & Baird, I. E. Further relations between primary production, chlorophyll, and particulate organic carbon. *Limnol. Oceanogr.* **7**, 42–47 (1962).
68. Xia, C. S., Qiao, F. L., Yang, Y. Z., Ma, J. & Yuan, Y. L. Three-dimensional structure of the summertime circulation in the Yellow Sea from a wave-tide-circulation coupled model. *J. Geophys. Res.* **111**, C11S03 (2006).
69. Chavez, F. P. et al. On the chlorophyll a retention properties of glass-fiber GF/F filters. *Limnol. Oceanogr.* **40**, 428–433 (1995).

70. Hedges, J. I. et al. Compositions and fluxes of particulate organic material in the Amazon River. *Limnol. Oceanogr.* **31**, 717–738 (1986).
71. Lee, S. & Fuhrman, J. A. Relationships between biovolume and biomass of naturally derived marine bacterioplankton. *Appl. Environ. Microb.* **53**, 1298–1303 (1987).
72. Falkowski, P. G. Rationalizing elemental ratios in unicellular algae. *J. Phycol.* **36**, 3–6 (2000).
73. Arrigo, K. R. Marine microorganisms and global nutrient cycles. *Nature* **437**, 349–355 (2005).
74. Nelson, D. M. et al. Particulate matter and nutrient distributions in the ice-edge zone of the Weddell Sea: relationship to hydrography during late summer. *Deep Sea Res.* **36**, 191–209 (1989).
75. Legendre, L. & Michaud, J. Chlorophyll a to estimate the particulate organic carbon available as food to large zooplankton in the euphotic zone of oceans. *J. Plankton Res.* **21**, 2067–2083 (1999).
76. Jakobsen, H. H. & Markager, S. Carbon-to-chlorophyll ratio for phytoplankton in temperate coastal waters: seasonal patterns and relationship to nutrients. *Limnol. Oceanogr.* **61**, 1853–1868 (2016).
77. Thomas, H., Ittekot, V., Osterroht, C. & Schneider, B. Preferential recycling of nutrients—the ocean's way to increase new production and to pass nutrient limitation? *Limnol. Oceanogr.* **44**, 1999–2004 (1999).
78. Middelburg, J. J. & Herman, P. M. J. Organic matter processing in tidal estuaries. *Mar. Chem.* **106**, 127–147 (2007).
79. Geider, R. J. Light and temperature dependence of the carbon to chlorophyll a ratio in microalgae and cyanobacteria: implications for physiology and growth of phytoplankton. *New Phytol.* **106**, 1–34 (1987).
80. Abdel-moati, A. R. Particulate organic matter in the subsurface chlorophyll maximum layer of the southeastern Mediterranean. *Oceanol. Acta* **13**, 307–315 (1990).
81. Geider, R. J., MacIntyre, H. L. & Kana, T. M. Dynamic model of phytoplankton growth and acclimation: responses of the balanced growth rate and the chlorophyll a:carbon ratio to light, nutrient-limitation and temperature. *Mar. Eco. Prog. Ser.* **148**, 187–200 (1997).
82. Beardall, J. & Giordano, M. Ecological implications of microalgal and cyanobacterial CO_2 concentrating mechanisms and their regulation. *Funct. Plant Biol.* **29**, 335–347 (2002).
83. Chen, C. T. A. Chemical and physical fronts in the Bohai, Yellow and East China seas. *J. Mar. Syst.* **78**, 394–410 (2009).
84. Tréguer, P. et al. Influence of diatom diversity on the ocean biological carbon pump. *Nature* **11**, 27–37 (2018).
85. Pedersen, M. F. & Borum, J. Nutrient control of algal growth in estuarine waters. Nutrient limitation and the importance of nitrogen requirements and nitrogen storage among phytoplankton and species of macroalgae. *Mar. Ecol. Prog. Ser.* **142**, 261–272 (1996).
86. Lomas, M. W. & Glibert, P. M. Comparisons of nitrate uptake, storage, and reduction in marine diatoms and flagellates. *J. Phycol.* **36**, 903–913 (2000).
87. Martiny, A. C., Vrugt, J. A., Primeau, F. W. & Lomas, M. W. Regional variation in the particulate organic carbon to nitrogen ratio in the surface ocean. *Glob. Biogeochem. Cycles* **27**, 727–731 (2013).
88. Golding, C. G., Lamboo, L. L., Beniac, D. R. & Booth, T. F. The scanning electron microscope in microbiology and diagnosis of infectious disease. *Sci. Rep.* **6**, 26516 (2016).
89. Dolgin, A. & Adolf, J. Scanning electron microscope of phytoplankton: achieving high-quality images through the use of safer alternative chemical fixatives. *J. Young Invest.* **37**, 1–9 (2019).
90. Geider, R. J. & La Roche, J. Redfield revisited: variability of C:N:P in marine microalgae and its biochemical basis. *Eur. J. Phycol.* **37**, 1–17 (2002).
91. Galbraith, E. D. & Martiny, A. C. A simple nutrient-dependence mechanism for predicting the stoichiometry of marine ecosystems. *Proc. Natl. Acad. Sci. USA* **112**, 8199–8204 (2015).
92. Marañón, E., Lorenzo, M. P., Cermeño, P. & Mouriño-Carballido, B. Nutrient limitation suppresses the temperature dependence of phytoplankton metabolic rates. *ISME J.* **12**, 1836–1845 (2018).
93. Francois, R. et al. Changes in the $\delta^{13}C$ of surface water particulate organic matter across the subtropical convergence in the SW Indian Ocean. *Glob. Biogeochem. Cycles* **7**, 627–644 (1993).
94. Kennedy, H. & Robertson, J. Variations in the isotopic composition of particulate organic carbon in surface waters along an 88°W transect from 67°S to 54°S. *Deep Sea Res.* **42**, 1109–1122 (1995).
95. Hedges, J. I., Keil, R. J. & Benner, R. What happens to terrestrial organic matter in the ocean? *Org. Geochem.* **27**, 195–212 (1997).
96. Johnston, A. M. The effect of environmental variables on ^{13}C discrimination by two marine phytoplankton. *Mar. Ecol. Prog. Ser.* **132**, 257–263 (1996).
97. Chou, W. C., Gong, G. C., Cai, W. H. & Tseng, C. M. Seasonality of CO_2 in coastal oceans altered by increasing anthropogenic nutrient delivery from large rivers: evidence from the Changjiang–East China Sea system. *Biogeosciences* **10**, 3889–3899 (2013).
98. Righetti, D., Vogt, M., Gruber, N., Psomas, A. & Zimmermann, N. E. Global pattern of phytoplankton diversity driven by temperature and environmental variability. *Sci. Adv.* **5**, eaar6253 (2019).
99. Chapman, C. C. et al. Defining Southern Ocean fronts and their influence on biological and physical processes in a changing climate. *Nat. Clim. Chang.* **10**, 209–219 (2020).
100. Bruno, J. F., Carr, L. A. & O'Connor, M. I. Exploring the role of temperature in the ocean through metabolic scaling. *Ecology* **96**, 3126–3140 (2015).
101. Barton, S. & Yvon-Durocher, G. Quantifying the temperature dependence of growth rate in marine phytoplankton within and across species. *Limnol. Oceanogr.* **64**, 2081–2091 (2019).
102. Goericke, R., Montoya, J. P. & Fry, B. Physiology of isotope fractionation in algea and cyanobacteria. in *Stable isotopes in ecology* (eds Lajtha, K. & Michener, B.) 187–221 (Blackwell Scientific Publications, 1994).
103. Farquhar, G. D., O'Leary, M. H. & Berry, J. A. On the relationship between carbon isotope discrimination and the intercellular carbon dioxide concentration in leaves. *J. Plant Physiol.* **9**, 121–137 (1982).
104. Berry, J. A. Studies of mechanisms affecting the fractionation of carbon isotopes in photosynthesis. in *Stable Isotopes in Ecological Research* (eds Rundel, P. W., Ehleringer, J. R. & Nagy, K. A.) 82–94 (Springer, 1989).
105. Mook, W. G., Bommerson, J. C. & Staverman, W. H. Carbon isotope fractionation between dissolved bicarbonate and gaseous carbon dioxide. *Earth Planet. Sci. Lett.* **22**, 169–176 (1974).
106. Boller, A. J., Thomas, P. J., Cavanaugh, C. M. & Scott, K. M. Low stable carbon isotope fractionation by coccolithophore RubisCO. *Geochim. Cosmochim. Acta* **75**, 7200–7207 (2011).
107. Boller, A. J., Thomas, P. J., Cavanaugh, C. M. & Scott, K. M. Isotopic discrimination and kinetic parameters of RubisCO from the marine bloom-forming diatom, *Skeletonema costatum*. *Geology* **13**, 33–43 (2015).
108. Paneth, P. & O'Leary, M. H. Carbon isotope effect on dehydration of bicarbonate ion catalyzed by carbonic anhydrase. *Biochemistry* **24**, 5143–5147 (1985).
109. Keeler, K. & Morel, F. M. M. A model of carbon isotopic fractionation and active carbon uptake in phytoplankton. *Mar. Ecol. Prog. Ser.* **182**, 295–298 (1999).
110. Raven, J. A. & Beardall, J. CO_2 concentrating mechanisms and environmental change. *Aquat. Bot.* **118**, 24–37 (2014).
111. Baird, M. E., Emsley, S. M. & Mcglade, J. M. Using a phytoplankton growth model to predict the fractionation model. *J. Plankton Res.* **23**, 841–848 (2001).
112. Burkhardt, S., Amoroso, G., Riebesell, U. & Sultemeyer, D. CO_2 and HCO_3^- uptake in marine diatoms acclimated to different CO_2 concentrations. *Limnol. Oceanogr.* **46**, 1378–1391 (2001).
113. Rost, B., Riebesell, U., Burkhardt, S. & Sultemeyer, D. Carbon acquisition of bloom-forming marine phytoplankton. *Limnol. Oceanogr.* **48**, 55–67 (2003).
114. Fielding, S. R. *Emiliania huxleyi* specific growth rate dependence on temperature. *Limnol. Oceanogr.* **58**, 663–666 (2013).
115. Krumhardta, K. M., Lovenduskib, N. S., Iglesias-Rodriguezc, M. D. & Kleypasd, J. A. Coccolithophore growth and calcification in a changing ocean. *Prog. Oceanogr.* **159**, 276–295 (2017).
116. Tortell, P. D. et al. Inorganic C utilization and C isotope fractionation by pelagic and sea ice algal assemblages along the Antarctic continental shelf. *Mar. Ecol. Prog. Ser.* **483**, 47–66 (2013).
117. Raven, J. A., Giordano, M., Beardall, J. & Maberly, S. C. Algal and aquatic plant carbon concentrating mechanisms in relation to environmental change. *Photosynth. Res.* **109**, 281–296 (2011).
118. Beardall, J., Griffiths, H. & Raven, J. A. Carbon isotope discrimination and the CO_2 accumulating mechanism in Chlorella emersonii. *J. Exp. Bot.* **33**, 729–737 (1982).
119. Kranz, S. A. et al. Low temperature reduces the energetic requirement for the CO_2 concentrating mechanism in diatoms. *New Phytol.* **205**, 192–201 (2014).
120. Rost, B., Zondervan, I. & Wolf-Gladrow, D. Sensitivity of phytoplankton to future changes in ocean carbonate chemistry: current knowledge, contradictions and research directions. *Mar. Ecol. Prog. Ser.* **373**, 227–237 (2008).
121. Deuser, W. G. Isotopic evidence for diminishing supply of available carbon during diatom bloom in the Black Sea. *Nature* **225**, 1069–1071 (1970).
122. Zeebe, R. E. & Wolf-Gladrow, D. CO_2 in *Seawater: Equilibrium, Kinetics, Isotopes* (Elsevier Science, 2001).
123. Wang, S. L., Yeager, K. M. & Li, W. Q. Carbon isotope fractionation in phytoplankton as a potential proxy for pH rather than for $[CO_2(aq)]$: observations from a carbonate lake. *Limnol. Oceanogr.* **61**, 1259–1270 (2016).
124. Gibbs, S. J. et al. Ocean warming, not acidification, controlled coccolithophore response during past greenhouse climate change. *Geology* **44**, 59–62 (2015).
125. Matoo, O. B., Lannig, G., Bock, C. & Sokolova, I. M. Temperature but not ocean acidification affects energy metabolism and enzyme activities in the blue mussel, *Mytilus edulis*. *Ecol. Evol.* **11**, 3366–3379 (2021).
126. Arar, E. J. & Collins, G. B. *Method 445.0 In Vitro Determination of Chlorophyll a and Pheophytin ain Marine and Freshwater Algae by Fluorescence* (United States Environmental Protection Agency, 1997).
127. Dickson, A.G., Sabine, C.L. & Christian, J.R. *Guide to Best Practices for Ocean CO_2 Measurements* (PICES Special Publication, 2007).

128. Huang, W. J., Wang, Y. C. & Cai, W. J. Assessment of sample storage techniques for total alkalinity and dissolved inorganic carbon in seawater. *Limnol. Oceanogr. Methods* **10**, 711–717 (2012).
129. Wang, S. Y. & Zhai, W. D. Regional differences in seasonal variation of air–sea CO_2 exchange in the Yellow Sea. *Cont. Shelf Res.* **218**, 104393 (2021).
130. Millero, F. J., Graham, T. B., Huang, F., Bustos-Serrano, H. & Pierrot, D. Dissociation constants of carbonic acid in sea water as a function of salinity and temperature. *Mar. Chem.* **100**, 80–94 (2006).
131. Dickson, A. G. Standard potential of the reaction: $AgCl(s) + 1/2H_2(g) = Ag(s) + HCl(aq)$, and the standard acidity constant of the ion HSO_4^- in synthetic sea water from 273.15 to 318.15 K. *J. Chem. Thermodyn.* **22**, 113–127 (1990).

Acknowledgements

This study was funded by the National Natural Science Foundation of China (41273083 (SK) and U1805242 (CTC)). The sampling survey was supported by the National Natural Science Foundation of China (grant number 41649901) via ship-time sharing projects during the Open Research Cruise conducted in Bohai and Yellow Seas by the R/V *Dongfanghong 2* (cruise number NORC2017-01). We appreciate the help of Li Chao (Department of Geological Oceanography, College of Ocean and Earth Sciences, Xiamen University) in SEM imaging and identification of phytoplankton species from the SEM photos. We are also grateful to the editors and two anonymous reviewers for critical comments that greatly improved the quality of the paper.

Author contributions

S.K. conceived and designed the study. Q.L. and H.W. collected the sample and performed the measurements. W.Z. contributed to the analyses. Y.V. and A.G. supported the data interpretation. Q.L. and S.K. wrote the paper. S.K. and C.T.A. secured funding. All authors reviewed and revised the paper.

Competing interests

The authors declare no competing interests.

Additional information

Supplementary information The online version contains supplementary material available at https://doi.org/10.1038/s43247-022-00627-y.

Correspondence and requests for materials should be addressed to Selvaraj Kandasamy.

Peer review information *Communications Earth & Environment* thanks John Beardall and the other, anonymous, reviewer(s) for their contribution to the peer review of this work. Primary Handling Editors: Annie Bourbonnais, Clare Davis, Heike Langenberg. Peer reviewer reports are available.

Reprints and permission information is available at http://www.nature.com/reprints

Publisher's note Springer Nature remains neutral with regard to jurisdictional claims in published maps and institutional affiliations.